

Sojourn probabilities in tubes and pathwise irreversibility for Itô processes

Julian Kappler* and Ronojoy Adhikari

DAMTP, Centre for Mathematical Sciences, University of Cambridge, Wilberforce Road, Cambridge CB3 0WA, UK

(Dated: October 11, 2021)

The sojourn probability of an Itô diffusion process, that is its probability to remain in the tubular neighborhood of a smooth path, is a central quantity in the study of path probabilities. Previous works considered the sojourn probability in the limit of vanishing tube radius, and employed the metric induced by the diffusion tensor, rather than that of the ambient space, to define the tube enclosing the smooth path. This presents two difficulties in experimentally measuring sojourn probabilities: first, the state-dependence of the diffusion tensor is not known a priori, and second, the limit has to be accessed through a sequence of measurements at finite tube radius. Here we circumvent these difficulties by obtaining a general expression for the sojourn probability of N -dimensional Itô processes in tubes whose radii are small but finite, and fixed by the metric of the ambient Euclidean space. The central quantity in our study is the rate at which trajectories leave the tube for the first time. This has an interpretation as a Lagrangian and can be measured directly in experiment. We find that this Lagrangian differs, in general, from the Onsager-Machlup Lagrangian and has a form not previously reported in the literature. We confirm our result by comparing to numerical simulations for a one-dimensional diffusion process with state-dependent diffusivity. For a one-dimensional example system, we then demonstrate that the most probable tube for a barrier crossing depends sensitively on the tube radius, and hence on the tolerated amount of fluctuations around the smooth reference path. Finally, we find that while in the limit of vanishing tube radius the ratio of sojourn probabilities for a pair of distinct paths is in general divergent, the same for a path and its time-reversal is always convergent and finite. This provides, in turn, a pathwise definition of irreversibility for Itô processes that is agnostic to the state-dependence of the diffusion tensor.

I. INTRODUCTION

A fundamental challenge in diffusive dynamics is to quantify the probability of a given trajectory in a meaningful way [1–16]. Apart from constituting a full description of the underlying stochastic dynamics, path probabilities are used in the context of rare events [17–23], or in stochastic thermodynamics, where the ratio of probabilities for a path and its time-reversed version characterizes irreversibility, and can be used to quantify entropy production [24–26].

For diffusive stochastic dynamics, as described by the Langevin equation, there exists a large body of literature on quantifying relative probabilities of stochastic trajectories [2–16]. If the noise term in the Langevin equation is state-independent, then relative path probabilities can be defined via the sojourn probability, i.e. the probability that a stochastic trajectory always remains within a finite-radius tube around a given twice continuously differentiable reference path. In that case, relative path probabilities can be defined as ratios of sojourn probabilities in the limit of vanishing time-independent tube radius, and are quantified by the Onsager-Machlup (OM) stochastic action Lagrangian [3, 4, 7–9, 27]. An advantage of this approach to path probabilities is that, while the probability of an individual trajectory vanishes, for finite tube radius the sojourn probability is positive. It can hence be measured directly, and indeed finite-radius

tubes were recently used to infer ratios of path probabilities experimentally [28].

However, often the noise in a Langevin equation is multiplicative, i.e. depends on the current state [29]. This is for example the case when the Langevin equation describes a slow reaction coordinate of a high-dimensional dynamical system [30–32], for stochastic dynamics with temperature gradients [33], or if hydrodynamic interactions are present [34–36]. For state-dependent noise, the limiting ratio of constant-radius tube probabilities in general does not yield meaningful results. Indeed, it has been shown that for multiplicative noise there is no translational invariant measure on the space of all paths [4], so that defining a probability density on that space is not possible, and comparing relative probabilities of individual paths not straightforward. Still, starting with the work of Freidlin and Wentzel [37], and Stratonovich [3], there have been several attempts to quantify relative path probabilities also in systems with multiplicative noise [6, 7]. However, these works, which can broadly be classified into two approaches, use definitions of the tube which are not practical from an experimental point of view. One approach is to define the tubular neighborhood using the metric induced by the diffusion tensor of the stochastic dynamics [37]. The tube is then a moving ellipsoid in \mathbb{R}^N , whose principal axes may vary along the reference path, which is the geometric center of mass of the ellipsoid. Another approach is to locally introduce a new coordinate system, with respect to which the diffusivity is state-independent [3, 7]. In this new coordinate system, the established theory for additive noise recovers the OM Lagrangian, which is then rewritten in

* jk762@cam.ac.uk

terms of the original coordinates, leading to an expression for ratios of path probabilities. The tube in the original coordinates is in this approach the inverse image of a constant-radius tube in the new coordinates. Since the relation between the two sets of coordinates is nonlinear, in the original coordinates the tube can have an in principal arbitrary geometrical shape, with a geometric center of mass that need not coincide with the reference path, as we show explicitly further below. In both approaches, the tube is therefore not a moving ball in Euclidean space, but an ellipsoid or more general geometrical structure. Importantly, in both cases the diffusivity tensor associated with the underlying stochastic dynamics needs to be known to even construct the tube. From an observational point of view it is of course desirable to consider a tube which can be constructed explicitly without first having to parametrize the underlying diffusive dynamics. In particular, the natural object to consider is a constant-radius tube with respect to the Euclidean metric of the ambient space, and hitherto no theory existed for that scenario.

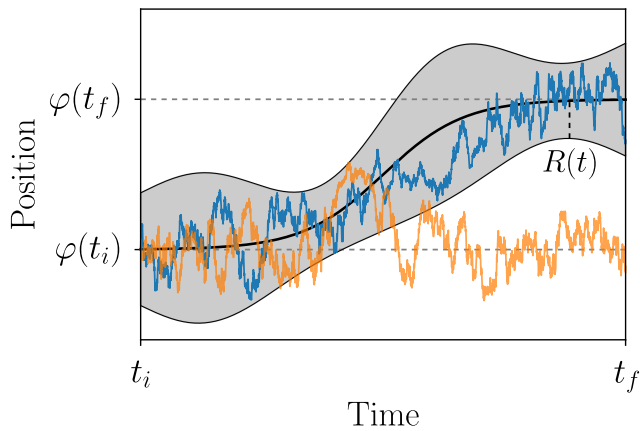


Figure 1. Illustration of the setup considered in this work. The black line depicts a reference path $\varphi(t)$ starting at $\varphi(t_i)$ and ending at $\varphi(t_f)$, as indicated by gray dashed lines. The gray shaded region depicts a tube with time-dependent radius $R(t)$ around φ , as indicated by the vertical dashed line. The blue curve is a realization of one-dimensional Langevin dynamics with multiplicative noise which remains within the tube until the final time, the orange curve represents a realization that leaves the tube before the final time t_f .

We here fill this gap, by providing a comprehensive theory of tube probabilities for diffusive dynamics with state-dependent diffusivity. We achieve this by establishing an expression for the sojourn probability for tubes with small-but-finite radius, which may vary along the reference path. The central quantity in our theory is the exit rate at which trajectories first leave the tube, and we present a series expansion of this exit rate in powers of the time-dependent tube radius.

Our theory for finite-radius tubes leads to a physical picture as to why the definition of ratios of path proba-

bilities is not straightforward for state-dependent diffusivity. Namely, because Langevin dynamics is at short length- and time scales dominated by the noise, as compared to the drift, for state-dependent diffusivity a path experiencing an, on average, larger diffusivity will always be infinitely more unlikely as compared to a path experiencing a lower average diffusivity. Limiting ratios of tube probabilities are therefore in general either zero or diverge, and finite nonzero limiting ratios for a pair of paths are only obtained if the tube radius is fine-tuned during the limiting procedure, in such a way that the dominating short-time noise contributions cancel.

We show that while limiting ratios of sojourn probabilities in general do not yield meaningful results, the ratio for a pair of forward and time-reverse reference path is always finite. This provides a pathwise definition of irreversibility for Itô processes that is agnostic to the state-dependence of the diffusion tensor, and which is related to classical measures of irreversibility and entropy production [25, 33, 38].

For the special case of a one-dimensional system, we derive explicit expressions for the exit rate describing the sojourn probability, and discuss several choices for the time-dependent tube radius. In particular we present an explicit formula for the sojourn probability of a constant-radius tube. We validate our theory by comparing to numerical simulations, and discuss explicitly the relation of the Stratonovich Lagrangian [3] to tubular exit rates. In the context of barrier crossing for a one-dimensional system, we furthermore find that the most probable tube depends sensitively on both the details of the time-dependence of the radius, and the size of the tube.

The present work provides a fundamentally new approach to quantifying and generalizing path probabilities for systems with state-dependent diffusivity. Because of its close relation to observables, our theory allows to extend, in an experimentally relevant way, any concept related to path probabilities, such as entropy production and most probable paths connecting an initial and a final point.

The remainder of this paper is structured as follows. In Sect. II we first discuss our general theory for N -dimensional Langevin dynamics. In Sect. III we consider the case of a one-dimensional system. We provide explicit expressions for the exit rate, discuss several possible choices for $R(t)$, and relate the Stratonovich Lagrangian to tubular exit rates. Finally, we discuss how the most probable tube connecting an initial and a final state can depend on the tube radius. In Sect. IV, we summarize our findings and discuss their further implications.

II. THEORY

In the present section, we discuss our general results for N -dimensional diffusive dynamics. For an N -dimensional coordinate $\mathbf{X}_t \equiv \mathbf{X}(t) \equiv (X_1(t), \dots, X_N(t))$, we consider

the Langevin equation given by [29, 39]

$$d\mathbf{X}_t = \mathbf{a}(\mathbf{X}_t, t) dt + \underline{\mathbf{b}}(\mathbf{X}_t, t) d\mathbf{W}_t, \quad (1)$$

where \mathbf{W}_t is the N -dimensional Wiener process, \mathbf{a} is the drift, and $\underline{\mathbf{b}}$ is the noise matrix, with components $a_i \equiv a_i(\mathbf{x}, t)$, $b_{ij} \equiv b_{ij}(\mathbf{x}, t)$. We interpret Eq. (1) in the Itô sense, results for other conventions are obtained from our results by modifying the drift term \mathbf{a} appropriately [39]. The stochastic dynamics defined by Eq. (1) can equivalently be described by the corresponding Fokker-Planck equation (FPE) [29, 39]

$$\partial_t P = -\nabla_i (a_i P) + \nabla_i \nabla_j (D_{ij} P), \quad (2)$$

where $P(\mathbf{x}, t)$ is the probability density for finding a particle \mathbf{X}_t at position \mathbf{x} and time t , by $\nabla_i \equiv \partial/\partial x_i$ we denote the partial derivative in the x_i -direction, and the components of the symmetric diffusion tensor $\underline{\mathbf{D}}$ are given by $D_{ij}(\mathbf{x}, t) \equiv b_{ik}(\mathbf{x}, t)b_{jk}(\mathbf{x}, t)/2$, where we use the Einstein sum convention for repeated indices. To denote time derivatives, we use the notation $\partial_t P$ and \dot{P} interchangeably.

A. The tubular ensemble

We consider the tubular ensemble, which consists of those realizations \mathbf{X}_t of the Langevin Eq. (1) that for times $t \in [0, t_f]$ remain within a time-dependent distance $R(t)$ to a continuous reference path $\varphi(t)$ [3–9, 40],

$$\mathcal{X}_R^\varphi(t) \equiv \{ \mathbf{X} \mid \|\mathbf{X}_s - \varphi(s)\| < R(s) \ \forall s \in [0, t] \}, \quad (3)$$

where the norm $\|\cdot\|$ used to quantify distances can be any norm on \mathbb{R}^N . The name tubular ensemble is used for \mathcal{X}_R^φ because a ball of radius $R(t)$ (defined with respect to the norm $\|\cdot\|$) with center $\varphi(t)$ is a tube in spacetime (\mathbf{x}, t) , see Fig. 1 for an illustration.

The corresponding sojourn probability

$$P_R^\varphi(t) \equiv P(\mathbf{X} \in \mathcal{X}_R^\varphi(t); \mathbf{X}_0 \sim P_i) \quad (4)$$

is the probability that a stochastic trajectory \mathbf{X} remains closer than a distance R to φ until time t ; for finite R this probability of course depends on the distribution of initial positions $\mathbf{X}_0 \sim P_i$ inside the tube. The decay of the sojourn probability can be described by $\alpha_R^\varphi(t)$, the instantaneous rate at which stochastic trajectories leave the tube for the first time, as

$$P_R^\varphi(t) = \exp \left[- \int_0^t ds \alpha_R^\varphi(s) \right]. \quad (5)$$

The sojourn probability is a functional of both the reference path $\varphi(t)$ and the function $R(t)$ which specifies the time-dependence of the radius, and is equivalently described by the functional

$$S[\varphi, R] \equiv \int_0^t ds \alpha_R^\varphi(s), \quad (6)$$

which we refer to as stochastic action because it describes experimentally observable sojourn probabilities.

As discussed in more detail at the end of this section and in App. A, for the Langevin Eq. (1), and considering a twice continuously differentiable reference path φ , as well as the standard Euclidean norm $\|\mathbf{x}\|_2 \equiv \sqrt{x_1^2 + x_2^2 + \dots + x_N^2}$ to define the tube, the exit rate can be expanded as a perturbation series for small $R(t)$, yielding

$$\mathcal{L}_R^\varphi(t) \equiv \alpha_R^\varphi(t) = \alpha_{\text{free}}^\varphi(t) + \alpha^{\varphi, (0)}(t) + \alpha^{\varphi, (2)} R^2(t) + \mathcal{O}(R^4(t)), \quad (7)$$

which defines the Lagrangian \mathcal{L}_R^φ , and where

$$\alpha_{\text{free}}^\varphi(t) \equiv \frac{f(\underline{\mathbf{D}}(\varphi(t), t))}{R^2(t)} \quad (8)$$

is the instantaneous steady-state free-diffusion exit rate out of an N -dimensional ball of radius $R(t)$ for Langevin dynamics with vanishing drift and a constant diffusion tensor $\underline{\mathbf{D}}(\varphi(t), t)$. For a symmetric matrix $\underline{\mathbf{M}}$, the function $f(\underline{\mathbf{M}})$ is defined as the smallest negative eigenvalue of the anisotropic Laplace operator in the unit ball with absorbing boundary conditions, and with anisotropy given by $\underline{\mathbf{M}}$. While at time t the free-diffusion exit rate Eq. (8) scales as $1/R^2(t)$ and only depends on $\underline{\mathbf{D}}(\varphi(t), t)$, the term $\alpha^{\varphi, (0)}(t)$ in Eq. (7) is of order $R^0(t)$ and depends on $\mathbf{a}(\varphi(t), t)$, $\underline{\mathbf{D}}(\varphi(t), t)$, as well as their spatial and temporal derivatives up to second order evaluated at $(\varphi(t), t)$. To derive Eq. (7) we assume that \dot{R}/R scales as R^0 . As we will see in our one-dimensional example further below, both $\alpha^{\varphi, (0)}$ and $\alpha^{\varphi, (2)}$ can depend on \dot{R}/R .

The Langevin Eq. (1) is on short length- and time scales dominated by the random noise term, which explains that for small radius the exit rate Eq. (7) is dominated by the instantaneous steady-state free-diffusion exit rate. This rate diverges as the radius approaches zero, which via Eq. (5) implies that the probability of any individual path vanishes. Because of this, the probability Eq. (5) at finite radius is the fundamental physical observable for diffusive dynamics. The expansion Eq. (7) allows to calculate this tube probability for small-but-finite time-dependent radius $R(t)$, and hence to quantify path probabilities for diffusive trajectories in an experimentally measurable way.

B. Asymptotic ratios of tube probabilities

Ratios of probabilities for individual paths can be defined for systems with a constant isotropic diffusion tensor $\underline{\mathbf{D}} \equiv D_0 \underline{\mathbf{1}} \equiv \text{const.}$, where D_0 is positive and $\underline{\mathbf{1}}$ denotes the unit matrix, and considering tubes of constant radius, $R(t) \equiv R_0 = \text{const.}$, with respect to the standard Euclidean norm [3–9, 27]. This is because the radius-dependent free-diffusion exit rate Eq. (8) is then independent of the path φ , so that the subleading-order

term $\mathcal{L}_{\text{OM}} \equiv \alpha^{\varphi,(0)}$ quantifies relative path probabilities. Indeed, for two paths φ, ψ , a stochastic action $S^{(0)}$ can be defined via [3–9, 27]

$$\frac{e^{-S^{(0)}[\varphi]}}{e^{-S^{(0)}[\psi]}} \equiv \lim_{R_0 \rightarrow 0} \frac{P_R^\varphi(t_f)}{P_R^\psi(t_f)}, \quad (9)$$

where $S^{(0)}[\varphi]$, which is a functional of the twice continuously differentiable path φ , is found to be

$$S^{(0)}[\varphi] = \int_0^{t_f} dt \mathcal{L}_{\text{OM}}(\varphi(t), \dot{\varphi}(t), t), \quad (10)$$

with the Onsager-Machlup (OM) Lagrangian

$$\mathcal{L}_{\text{OM}}(\varphi, \dot{\varphi}) \equiv \alpha^{\varphi,(0)} = \frac{1}{4D_0} [\dot{\varphi} - \mathbf{a}(\varphi)]^2 + \frac{1}{2} \nabla \cdot \mathbf{a}(\varphi). \quad (11)$$

For additive isotropic noise, ratios of path probabilities can thus be defined as limits of constant-radius sojourn probabilities, and the OM Lagrangian quantifies such ratios [3–8, 27].

For a state-dependent diffusion tensor, however, the limit in Eq. (9) in general does not yield meaningful results. In that case, it follows from substituting Eqs. (7), (8), into Eq. (5) that

$$\begin{aligned} \ln \frac{P_R^\varphi(t_f)}{P_R^\psi(t_f)} &= - \int_0^{t_f} ds \left[\frac{f(\underline{\mathbf{D}}(\varphi(s), s))}{R_\varphi^2(s)} - \frac{f(\underline{\mathbf{D}}(\psi(s), s))}{R_\psi^2(s)} \right] \\ &\quad - \int_0^{t_f} ds \left[\alpha^{\varphi,(0)}(s) - \alpha^{\psi,(0)}(s) \right] + \mathcal{O}(R^2) \end{aligned} \quad (12)$$

where we allow for different time-dependent radius R_φ, R_ψ , along the paths φ, ψ , while still assuming that both radii are of the same order, $\mathcal{O}(R_\varphi) = \mathcal{O}(R_\psi) \equiv \mathcal{O}(R)$ at each time t . From Eq. (12) it is clear that in general the difference of the free-diffusion exit rates does not vanish, so that in the limit $R_\varphi(t), R_\psi(t) \rightarrow 0$ for all t the expression Eq. (12) diverges. We remark that of course for multiplicative noise the subleading-order term $\alpha^{\varphi,(0)}$ is in general not identical to the OM Lagrangian Eq. (11).

Equation (12) shows that for state-dependent diffusivity, considering ratios of tube probabilities in the limit of vanishing tube radius leads to divergences. Physically speaking, in a region with low diffusivity a particle is less likely to diffuse away from a reference path, as compared to a region with large diffusivity. The leading-order contribution to the small-radius sojourn probability is thus path dependent, and depends both on the local diffusivity along the path and the current tube radius. This asymptotic behavior of the sojourn probability gives an intuitive picture for the mathematical statement that the measure induced by Langevin dynamics with multiplicative noise on the space of all continuous paths is not absolutely continuous with respect to a quasi translation invariant measure on that space [4].

However, from Eq. (12) it is also evident that by choosing a path-dependent radius $R_\varphi(t) = C\sqrt{f(\underline{\mathbf{D}}(\varphi(t), t))}$, with a constant C , the leading order terms do cancel and the limit of vanishing tube radius, $C \rightarrow 0$, is finite. In this scenario, the radius is locally chosen such that the free-diffusion exit rate is independent of the path and Eq. (9) can be used to define a Lagrangian $\mathcal{L} \equiv \alpha^{\varphi,(0)}$. We want to emphasize three points in the context of this construction. First, one has to be aware that by effectively scaling away the leading-order differences in the asymptotic exit rate, ratios of path probabilities are in this scenario not directly related to what one would naturally measure in an experiment, namely the exit rate from a constant-radius tube with respect to the underlying Euclidean metric. In fact, to measure in an experiment the exit rate from a tube of radius $R_\varphi(t) = C\sqrt{f(\underline{\mathbf{D}}(\varphi(t), t))}$, the diffusion tensor $\underline{\mathbf{D}}$ needs to be known along the path φ to evaluate R_φ . Second, the construction presented in this paragraph is not the same as defining a tube via the metric induced by $\underline{\mathbf{D}}$ [37]. We here consider a ball in Euclidean space, with its radius rescaled along the trajectory so as to produce the same steady-state free-diffusion exit rate everywhere. A tube with respect to the metric induced by the diffusion tensor, on the other hand, corresponds to a moving ellipsoid in \mathbb{R}^N , whose principal axes vary along the reference path in such a way that the steady-state free-diffusion exit rate remains constant. Only for one-dimensional systems, $N = 1$, where ellipsoids and balls are identical and simply intervals, do these two constructions lead to the same tube. Third, the Lagrangian obtained by choosing a radius $R = C\sqrt{f(\underline{\mathbf{D}}(\varphi))}$ is not identical to the standard Lagrangian for multiplicative noise, which was originally derived by Stratonovich [3]. For a one-dimensional system we show this explicitly in Sect. III, where we also demonstrate how the Stratonovich Lagrangian is related to tubular exit rates.

The difficulties and ambiguities in extending the vanishing-radius limit of tube probabilities Eq. (9) to systems with multiplicative noise, together with the fact that any individual path has vanishing probability, suggests that instead of considering the limit $R \rightarrow 0$, focus should be put on the finite-radius sojourn probability Eq. (5) which describes observable events of positive probability.

However, note that while in general the log-ratio Eq. (12) diverges in the limit of vanishing tube radius, an important exception is the case where ψ, R_ψ are the time reverse of $\varphi, R_\varphi \equiv R$, i.e. where $\psi(t) \equiv \overleftarrow{\varphi}(t) \equiv \varphi(t_f - t)$, $R_\psi(t) \equiv R(t_f - t)$, and where we assume that for the reverse path also all explicit time-dependences in $\mathbf{a}, \underline{\mathbf{D}}$ are reversed (as is customary when considering irreversibility in stochastic thermodynamics [25, 26]). The leading

order terms in Eq. (12) then cancel and we obtain

$$\lim_{R \rightarrow 0} \ln \frac{P_R^\varphi(t_f)}{P_R^\leftarrow(t_f)} = - \int_0^{t_f} ds \left[\alpha^{\varphi, (0)}(s) - \alpha^{\leftarrow, (0)}(s) \right], \quad (13)$$

where the limit is considered pointwise, i.e. $R(t) \rightarrow 0$ for all t . The limiting ratio of sojourn probabilities for a pair of forward and reverse path is thus generally finite. We emphasize again that although $\alpha^{\varphi, (0)}(s)$ scales as R^0 , it can still depend on the exact form of R via \dot{R}/R , as we will see in our explicit one-dimensional example in Sect. III.

C. Most probable tubes and instantons

One application of path probabilities is determining the most probable path, also called instanton [4, 15]. However, since any individual path has vanishing probability, an object of more practical relevance than the instanton is the reference path which maximizes the sojourn probability for a finite-radius tube. From Eqs. (5), (6), we see that for a given time-dependent tube radius R_φ , which may depend on the path as indicated by the subscript, the most probable tube, with corresponding reference path φ^* connecting an initial position \mathbf{x}_0 at time $t = 0$ and a final position \mathbf{x}_f at time $t = t_f$, is obtained by minimizing the action Eq. (6),

$$\varphi^* \equiv \underset{\varphi}{\operatorname{argmin}} S[\varphi, R_\varphi], \quad (14)$$

where the minimization is over all continuous paths which fulfill $\varphi(0) = \mathbf{x}_0$, $\varphi(t_f) = \mathbf{x}_f$. After φ^* has been obtained, the finite sojourn probability to observe any trajectory that remains within the tube is calculated via Eq. (5).

An instanton may be defined from Eq. (14) as most probable tube in the limit of vanishing radius; the result of course depends on the exact form of $R_\varphi(t)$. For additive noise with a constant isotropic diffusivity tensor $\underline{D} \equiv D_0 \underline{1} \equiv \text{const.}$, and a constant radius, $R(t) \equiv R_0 = \text{const.}$, the limit $R_0 \rightarrow 0$ in Eq. (14) is equivalent to finding a path φ^* that minimizes the OM action Eq. (10). For the general Langevin Eq. (1) with multiplicative noise, we see from Eqs. (7), (8), that in the limit of vanishing time-independent tube radius, the instanton is in general the path which minimizes the average free-diffusion exit rate along the path. Thus, because diffusive dynamics is on short length- and time scales dominated by the random noise term in Eq. (1), for a generic Langevin equation the drift term is completely irrelevant for the most probable path.

D. Exit rate in terms of FP spectrum

To derive the perturbation series Eq. (7) for the exit rate, we consider the equivalent description of the

stochastic process Eq. (1) inside the tube via the Fokker-Planck equation (FPE) [29, 39]

$$\partial_t P_R^\varphi = -\nabla_i (a_i P_R^\varphi) + \nabla_i \nabla_j (D_{ij} P_R^\varphi), \quad (15)$$

where as before the components of the diffusion tensor \underline{D} are given by $D_{ij}(\mathbf{x}, t) \equiv b_{ik}(\mathbf{x}, t)b_{jk}(\mathbf{x}, t)/2$, and we use the Einstein sum convention for repeated indices. The time-dependent spatial domain for Eq. (15) is given at time t by

$$\mathbf{x} \in B_R^\varphi(t) \equiv \{ \mathbf{x} \mid \|\mathbf{x} - \varphi(t)\|_2 < R(t) \}, \quad (16)$$

as illustrated by the grey shaded area in Fig. 1. The solution to the FPE is subject to absorbing boundary conditions at the tube boundary, $P_R^\varphi(\mathbf{x}, t) = 0$ for all $\mathbf{x} \in \partial B_R^\varphi(t)$, so that $P_R^\varphi(\mathbf{x}, t)$ describes the distribution of those trajectories that have never left the tube until time t . Note that in Eq. (16) we consider the standard Euclidean norm, so that B_R^φ describes a moving ball in \mathbb{R}^N , with instantaneous radius $R(t)$ and center $\varphi(t)$.

To obtain Eq. (7), we use the same strategy as in a recent derivation [27] of finite-radius tubular exit rates for Langevin dynamics with isotropic additive diffusivity $\underline{D} = D_0 \underline{1}$, where D_0 is a positive scalar and $\underline{1}$ is the unit matrix. In the following, we provide a short summary of the derivation, more details can be found in App. A and Ref. [27]. Our derivation assumes that φ is twice continuously differentiable, and that \dot{R}/R scales as R^0 ; furthermore we use the standard Euclidean norm in \mathbb{R}^N to define the tube. To derive Eq. (7), we first introduce a dimensionless coordinate system that moves along the tube center; this removes the time-dependence of the boundary conditions. In the new coordinate system the FPE is subsequently projected onto the instantaneous eigenbasis $\tilde{\rho}_n$ of the FP operator, with corresponding eigenvalues $-\tilde{\lambda}_n$. In this eigenbasis, an approximate solution of the FPE for small tube radius is derived using an approach similar to time-dependent perturbation theory in quantum mechanics [41]. This solution is, after an initial relaxation timescale $\tau_{\text{rel}} \sim R(0)^2$, dominated by the decay of the slowest-decaying eigenfunction.

Once Eq. (15) is solved with absorbing boundary conditions, the sojourn probability up to time t is the survival probability, and obtained as a spatial integral over the solution of the FPE as

$$P_R^\varphi(t) = \int_{B_R^\varphi(t)} d^N \mathbf{x} P_R^\varphi(\mathbf{x}, t). \quad (17)$$

From this in turn we obtain the instantaneous exit rate $\alpha_R^\varphi(t)$ at which stochastic trajectories leave the tube for the first time, via

$$\alpha_R^\varphi(t) = -\frac{\dot{P}_R^\varphi(t)}{P_R^\varphi(t)}. \quad (18)$$

From this, the exit rate Eq. (7) then follows, and in App. A we derive expressions for f , $\alpha^{\varphi, (0)}$, $\alpha^{\varphi, (2)}$, in terms of the instantaneous spectrum $(-\tilde{\lambda}_n, \tilde{\rho}_n)$ of the dimensionless FP operator. In particular, we show that the equation for f at time t only depends on $\underline{D}(\varphi(t), t)$.

III. ONE-DIMENSIONAL SYSTEMS

A. Model

We now consider a one-dimensional system, given by a particle coupled to a heat bath and subject to an external force. In the limit of large friction, inertial effects can be neglected and the dynamics of the particle trajectory X_t is described by the Itô equation [42, 43]

$$dX_t = \left(\mu(X_t, t)F(X_t, t) + \frac{1}{2}(\partial_x D)(X_t, t) \right) dt + \sqrt{2D(X_t, t)} dW_t, \quad (19)$$

where $F(x, t)$ is the external force, and the mobility $\mu(x, t)$ and diffusion coefficient $D(x, t)$ are related via $\beta D(x, t) = \mu(x, t)$ with $\beta^{-1} = k_B T$ the thermal energy.

Equation (19) is the Langevin Eq. (1) for $N = 1$, with $a \equiv \mu F + \partial_x D/2$ and $b \equiv \sqrt{2D}$, and the corresponding FPE (15) has the form

$$\partial_t P_R^\varphi = -\partial_x \left[\left(\mu F + \frac{1}{2}(\partial_x D) \right) P_R^\varphi \right] + \partial_x^2 (D P_R^\varphi). \quad (20)$$

B. Exit rate

In App. C we explicitly calculate the FP spectrum for $N = 1$ and evaluate the exit rate Eq. (7) to order R^2 . The first two terms are

$$\alpha_{\text{free}}^\varphi(t) = \frac{\pi^2}{4} \frac{D(\varphi(t))}{R(t)^2} \quad (21)$$

and

$$\mathcal{L}^{\varphi, (0)} \equiv \alpha^{\varphi, (0)} = \frac{1}{4D} [\dot{\varphi} - D\beta F]^2 + \frac{1}{2} D\beta \partial_x F + \frac{1}{4} (\partial_x D)\beta F + \frac{\pi^2}{24} \partial_x^2 D - \frac{\pi^2}{16} \frac{(\partial_x D)^2}{D} + \frac{\partial_x D}{4D} \dot{\varphi} - \frac{1}{2} \frac{\dot{R}}{R}, \quad (22)$$

where D , F and their derivatives are evaluated at $(x, t) \equiv (\varphi(t), t)$, the radius is in general time-dependent, $R \equiv R(t)$, and may depend on φ , and where we assume that \dot{R}/R scales as R^0 . The quadratic contribution $\alpha^{\varphi, (2)}$ to the exit rate Eq. (7) is given App. C. The Lagrangian Eq. (22) is different from those derived for multiplicative noise found in the literature [3–9, 16]. The relevance of our result $\mathcal{L}^{\varphi, (0)}$ is that it appears as a term in the perturbative expansion of the exit rate Eq. (7), and hence is a physical observable.

As discussed in Sect. II A, for two paths φ , ψ the log-ratio of tube probabilities Eqs. (12) in general diverges as $R \rightarrow 0$. However, if for the second path we consider the time reverse of φ , i.e. $\psi(t) \equiv \overleftarrow{\varphi}(t) = \varphi(t_f - t)$, and also reverse all explicit time-dependences of D , F , R , then from Eqs. (13), (22), we obtain

$$\lim_{R \rightarrow 0} \ln \frac{P_R^\varphi(t_f)}{P_R^{\overleftarrow{\varphi}}(t_f)} = - \int_0^{t_f} dt \left[(\beta F)|_{\varphi(t)} \dot{\varphi}(t) \right] - 2 \lim_{R \rightarrow 0} \left(\ln \frac{D(\varphi)}{R^2} \Big|_{t=t_f} - \ln \frac{D(\varphi)}{R^2} \Big|_{t=0} \right), \quad (23)$$

The first term on the right-hand side is the familiar formula for the entropy production along the trajectory φ [25, 33, 38]. The second term on the right-hand side is a boundary term; if the diffusivity is independent of time, and the tube radius depends on time via a spatial function evaluated along the path, i.e. if $R(t) \equiv R_\varphi(t)$ is of the form $R(\varphi(t))$, then for a closed loop φ the boundary term vanishes. In that case, which includes the scenario of a constant tube radius $R(t) \equiv R_0 = \text{const.}$, the lim-

iting ratio of tube probabilities Eq. (23) along a closed path is equal to the medium entropy production along φ [25, 33].

We now discuss two particular choices for the time-dependent radius, namely the scenarios of constant radius and constant free-diffusion exit rate. Subsequently we relate the one-dimensional Stratonovich stochastic action Lagrangian [3] to tubular exit rates.

For the numerical examples with which we illustrate our results, we consider a force originating from a potential U as $F(x) = -(\partial_x U)(x)$, where for $U(x)$ we use a quartic double well with typical length scale L ,

$$U(x) = U_0 \left[\left(\frac{x}{L} \right)^2 - 1 \right]^2, \quad (24)$$

and barrier height $\beta U_0 = 2$; this potential is shown in Fig. 2 (a). We furthermore consider a diffusivity profile

$$D(x) = \frac{D_0}{4} \left[5 - \cos \left(\pi \frac{x}{L} \right) \right], \quad (25)$$

resulting in a diffusivity $D(x = \pm L) = D_0$ at the potential minima and $D(x = 0) = 3D_0/2$ at the barrier top. This diffusivity profile is shown in Fig. 2 (b), for our numerical results we use $D_0 = L^2/\tau_D$, so that $\tau_D = L^2/D_0$.

For the reference path φ we choose a barrier crossing path which at time $t_i = 0$ starts at $x = -L$ and at time $t_f = \tau_D$ ends at $x = L$, and which is parametrized as

$$\varphi(t) = \frac{L}{\arctan(\kappa/2)} \arctan \left[\kappa \cdot \left(\frac{t - t_f/2}{\tau_D} \right) \right], \quad (26)$$

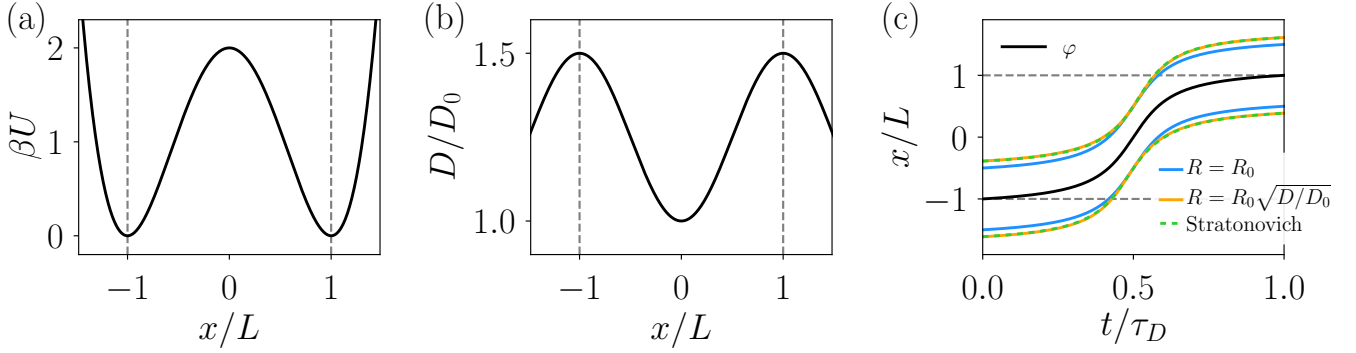


Figure 2. Potential, diffusivity, and path considered in the numerical examples in Sect. III. Subplot (a) shows the quartic double well potential Eq. (24) for barrier height $\beta U_0 = 2$. Subplot (b) shows the diffusivity profile Eq. (25). In subplot (c), we show the reference path φ , defined in Eq. (26). Around the reference path, we plot the boundaries of the respective tubes for the three scenarios considered in Sect. IIIB. For better visibility, all tube radii are increased by a factor of 5 for the plot. In all subplots, gray dashed lines denote two potential barrier minima $x = \pm L$.

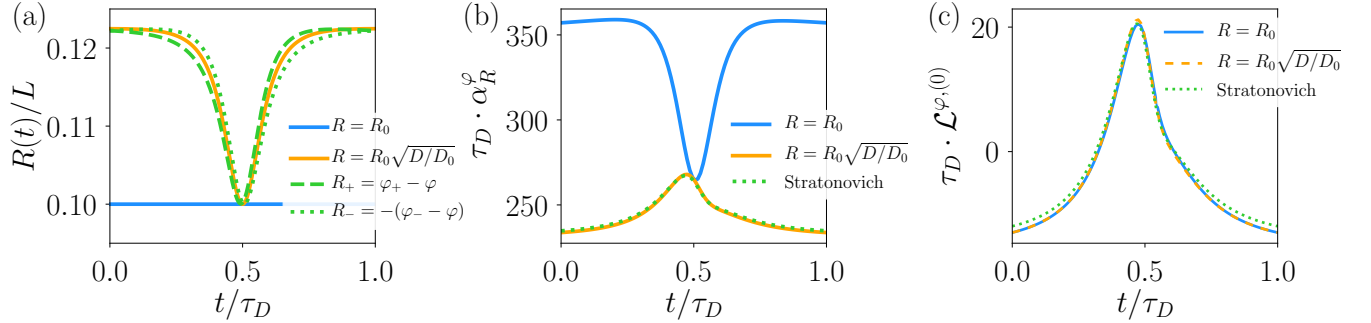


Figure 3. Tube radius and exit rates for the one-dimensional example system considered in Sect. III. Subplot (a) shows the time-dependent tube radius for constant tube radius (scenario 1; blue solid line), constant free-diffusion exit rate (scenario 2; orange solid line), and the distance from the reference path to the interval bounds for the Stratonovich construction (scenario 3; green dashed and dotted lines). For all scenarios, we use $R_0/L = 0.1$. Subplot (b) shows the perturbative exit rate Eq. (7) to order R^0 for constant tube radius (scenario 1; blue solid line), constant free-diffusion exit rate (scenario 2; orange solid line), and the Stratonovich construction (scenario 3; green dotted line). Subplot (c) shows $\mathcal{L}^{\varphi,(0)} \equiv \alpha^{\varphi,(0)}$, the first correction to the steady-state free-diffusion exit rate, for the three scenarios considered in subplot (b).

where for κ , which controls the maximal barrier crossing speed, we use $\kappa = 10$. The reference path Eq. (26) is illustrated in Fig. 2 (c).

Scenario 1: Constant tube radius. For a tube with constant radius, $R(t) \equiv R_0 = \text{const.}$, we obtain from Eqs. (21), (22), that

$$\alpha_{\text{free}}^{\varphi} = \frac{\pi^2 D(\varphi)}{4 R_0^2}, \quad (27)$$

$$\begin{aligned} \mathcal{L}_1^{\varphi,(0)} = & \frac{1}{4D} [\dot{\varphi} - D\beta F]^2 + \frac{1}{2} D\beta \partial_x F + \frac{1}{4} (\partial_x D)\beta F \\ & + \frac{\pi^2}{24} \partial_x^2 D - \frac{\pi^2}{16} \frac{(\partial_x D)^2}{D} + \frac{\partial_x D}{4D} \dot{\varphi}. \end{aligned} \quad (28)$$

Equation (27), which for small enough tube radius is the dominant contribution to the exit rate, is proportional to $D(\varphi(t), t)$ and hence path-dependent. In Fig. 3 (b) we show the exit rate Eq. (7) to order R^0 , evaluated along the path Eq. (26) for a tube radius $R_0/L = 0.1$. We

observe that the exit rate is significantly smaller when the path is close to the barrier top, where the diffusivity profile shown in Fig. 2 (b) displays a smaller value as compared to the potential wells $x = \pm L$. This indicates that the radius $R_0/L = 0.1$ is so small that the exit rate Eq. (7) is already dominated by the free-diffusion contribution Eq. (27) which is proportional to D . Indeed, by comparing the magnitude of the total exit rate to order R^0 , shown in Fig. 3 (b), to the typical magnitude of the order- R^0 term Eq. (28), plotted in Fig. 3 (c), we conclude that $\mathcal{L}_1^{\varphi,(0)}$ only contributes about 10% of the value of the total exit rate in subplot (b). In App. C4 we show, by comparison to numerically simulated tubular exit rates, that for the present system and tube considered, the perturbative exit rate Eq. (7) to order R^0 perfectly describes the numerically measured exit rate, so that for the small radius $R_0/L = 0.1$ the two terms Eqs. (27), (28) fully characterize the actual the exit rate.

Scenario 2: Constant free-diffusion exit rate. From

Eqs. (12), (27), we see that for constant tube radius the log-ratio of tube probabilities in general diverges as $R_0 \rightarrow 0$. As discussed in Sect. IIB, this divergence can be avoided by choosing a path-dependent tube radius $R(t) \equiv R(\varphi(t)) \equiv R_0 \sqrt{D(\varphi(t))/D_0}$, which for one-dimensional systems is equivalent to defining the tube with respect to the metric induced by the diffusivity tensor corresponding to the FP Eq. (2) [37]. In this scenario, we obtain from Eqs. (7), (22), that

$$\alpha_{\text{free}}^\varphi = \frac{\pi^2 D_0}{4 R_0^2} \equiv \text{const.} \quad (29)$$

$$\begin{aligned} \mathcal{L}_2^{\varphi,(0)} &= \frac{1}{4D} [\dot{\varphi} - D\beta F]^2 + \frac{1}{2} D\beta \partial_x F + \frac{1}{4} (\partial_x D)\beta F \\ &+ \frac{\pi^2}{24} \partial_x^2 D - \frac{\pi^2}{16} \frac{(\partial_x D)^2}{D}. \end{aligned} \quad (30)$$

By construction, the free-diffusion exit rate Eq. (29) is now independent of the path and constant as a function of time. In Fig. 3 (a), we show the time-dependent tube radius $R(t)$ for $R_0/L = 0.1$ and the example system Eqs. (24), (25), (26). In Fig. 3 (b) we show the corresponding theoretical exit rate Eq. (7) to order R^0 ; as we show in App. C 4 by comparison to numerical simulations of the exit rate, higher order terms are irrelevant for the small tube radius considered here. Figure 3 (b) clearly shows that the total exit rate varies on a much smaller scale as compared to the constant-radius exit rate from scenario 1. In Fig. 3 (c) we compare the Lagrangians Eqs. (28), (30) for scenarios 1 and 2. While overall the Lagrangians are rather similar, they deviate from each other for $t/\tau_D \approx 0.5$, when the path is close to the barrier top.

Turning to limiting ratios of tube probabilities for two paths φ, ψ , we note that by construction the limit $R_0 \rightarrow 0$ of Eq. (12) is finite in the present scenario, and yields

$$\lim_{R_0 \rightarrow 0} \ln \frac{P_R^\varphi(t_f)}{P_R^\psi(t_f)} = - \int_0^{t_f} ds \left[\mathcal{L}_2^{\varphi,(0)}(s) - \mathcal{L}_2^{\psi,(0)}(s) \right]. \quad (31)$$

We emphasize again that this ratio compares asymptotic tube probabilities for tubes which have a different time-dependent radius along the two paths φ, ψ .

Scenario 3: Stratonovich Lagrangian. Both Lagrangians Eqs. (28), (30), are different from the Lagrangian for multiplicative noise originally derived by Stratonovich [3], which in our notation reads

$$\mathcal{L}_S^\varphi = \frac{1}{4D} [\dot{\varphi} - D\beta F]^2 - \frac{1}{4} (\partial_x D)\beta F + \frac{1}{2} \partial_x [D\beta F]. \quad (32)$$

We now demonstrate that this Lagrangian corresponds to an exit rate from a moving interval which is not centered at the path φ , and which has a time-dependent radius that is to leading order identical to the one from scenario 2. To obtain Eq. (32), we introduce a new coordinate

system $y(x) \equiv \Phi(x)$ defined by

$$\frac{d\Phi}{dx} = \frac{1}{\sqrt{D(x)/D_0}}. \quad (33)$$

Transforming the 1D FPE to the y -coordinate leads to $\partial_t P_Y = -\partial_y (D_0 \beta F_Y P_Y) + D_0 \partial_y^2 P_Y$, where $P_Y(y, t) \equiv \sqrt{D(x)/D_0} P(x, t)$, $F_Y(y) \equiv \sqrt{D(x)/D_0} F(x)$, with $x = \Phi^{-1}(y)$. The coordinate transformation Eq. (33) locally stretches space where diffusivities are low, and locally compresses space where diffusivities are large, resulting in a constant diffusivity D_0 with respect to the y -coordinate, as was remarked by Ito [7]. The Stratonovich Lagrangian now follows by considering a tube with constant radius R_0 in the y -coordinate around the path $\varphi_Y(t) \equiv \Phi(\varphi(t))$. Since the diffusivity is constant in this coordinate system, the theory for stochastic dynamics with additive noise is applicable, for which the first correction to freely-diffusive exit from the tube is given by the OM Lagrangian Eq. (11) [27]. Expressing the resulting exit rate back in the original x -coordinates yields

$$\alpha_{R_0}^\varphi = \frac{\pi^2 D_0}{4 R_0^2} + \mathcal{L}_S^\varphi + \mathcal{O}(R_0^2) \quad (34)$$

with the Stratonovich Lagrangian Eq. (32). In summary, \mathcal{L}_S^φ is obtained by performing a nonlinear coordinate transformation Φ , considering a constant-radius tube in the new coordinates, and transforming the resulting expression for the exit rate back to the original coordinates. Importantly, a tube centered around $\Phi(\varphi(t))$ in the y -coordinate need not correspond to a tube centered around $\varphi(t)$ in the x -coordinate. More explicitly, at time t a tube of radius R_0 in the y -coordinate is in the x -coordinate bounded by the two points $\varphi_\pm(t) \equiv \Phi^{-1}(\Phi(\varphi(t)) \pm R_0)$. The center $\varphi_c(t) \equiv (\varphi_+(t) + \varphi_-(t))/2$ and radius $R(t) \equiv (\varphi_+(t) - \varphi_-(t))/2$ of this one-dimensional ball are given by

$$\varphi_c(t) = \varphi(t) + \frac{1}{4} \frac{\partial_x D|_{x=\varphi(t)}}{D_0} R_0^2 + \mathcal{O}(R_0^4), \quad (35)$$

$$R(t) = \left[\sqrt{\frac{D}{D_0}} R_0 + \frac{1}{12} \frac{\partial_x^2 D}{D_0} \sqrt{\frac{D}{D_0}} R_0^3 \right] \Big|_{x=\varphi(t)} + \mathcal{O}(R_0^5). \quad (36)$$

Equations (35), (36), are to leading order identical to tube center and radius from scenario 2, but contain additional higher-order terms.

We return to the example system Eqs. (24), (25), (26), and consider a tube of constant radius $R_0/L = 0.1$ in the y -coordinate. In Fig. 3 (a) we show the distance from $\varphi(t)$ to either of the two tube boundaries in the x -coordinate, i.e. $R_\pm(t) \equiv \pm(\varphi_\pm(t) - \varphi(t))$. The two curves R_\pm clearly disagree with each other, showing that the tube is in the x -coordinate not centered at φ . Both R_\pm behave similar to the tube radius from scenario 2, which according to Eq. (36) is their leading order behavior. Indeed, also in Fig. 3 (b), where we show the total exit rate Eq. (34)

to order R^0 , the exit rates from scenarios 2 and 3 look very similar. However, subtracting from the exit rate the free-diffusion contributions, which according to Eqs. (29), (34), are equal, we observe in Fig. 3 (c) that the order- R^0 Lagrangians from scenario 2 and 3, Eqs. (30), (32), clearly deviate from each other, most prominently at the beginning and the end of the path, i.e. for $t/\tau_D \lesssim 0.3$ and $t/\tau_D \gtrsim 0.7$.

We now consider ratios of tube probabilities for two paths φ , ψ for scenario 3. By construction, the free-diffusion exit rates are equal for any two paths, so that we obtain

$$\lim_{R_0 \rightarrow 0} \ln \frac{P_R^\varphi(t_f)}{P_R^\psi(t_f)} = - \int_0^{t_f} ds \left[\mathcal{L}_S^\varphi(s) - \mathcal{L}_S^\psi(s) \right]. \quad (37)$$

We emphasize that while in both scenarios 2 and 3 the ratio of tube probabilities is well-defined in the limit $R_0 \rightarrow 0$, the resulting stochastic Lagrangians differ. This highlights that limiting ratios of tube probabilities depend on the detailed nature of the tube. However, if we consider for ψ the reverse of φ , i.e. $\psi = \overleftarrow{\varphi}$, then from Eq. (37) we recover Eq. (23) without the boundary term.

C. Most probable tube

We now consider the most probable tube for the example system Eqs. (24), (25), and the three scenarios discussed in the previous section. For each scenario, we obtain the most probable tube for a barrier-crossing transition from $\varphi(0) = -L$ to $\varphi(t_f) = L$ in one unit of the diffusive time scale, $t_f = \tau_D$, by minimizing the action functional, as defined by Eq. (14). In Fig. 4 we compare the resulting most probable reference paths φ^* .

For constant tube radius $R \equiv R_0/L = 0.1$, the most probable reference path φ^* (blue solid line) remains on the barrier top $x = 0$ for most of the transition time. This is because the action is, for the small radius considered here, dominated by the free-diffusion exit rate Eq. (27), which is proportional to the diffusivity. Because the diffusivity profile Eq. (25) features a local minimum at $x/L = 0$, the free-diffusion exit rate is minimal there. Notably, it follows that for tubes of small constant radius the most probable tube is only weakly influenced by the Lagrangian Eq. (28), and in particular is much more influenced by the diffusivity profile $D(x, t)$ as compared to the force $F(x, t)$.

For constant free-diffusion exit rate, $R(t) \equiv R_0 \sqrt{D(\varphi(t))/D_0}$, the most probable tube shown in Fig. 4 remains within the potential wells most of the time, and crosses the barrier rather quickly without stopping at the barrier top; this is in sharp contrast to the constant-radius result. Because in the present scenario the free-diffusion term Eq. (29) is independent of the path, the extremum of the action is determined by the subleading-order contribution Eq. (30). Indeed, the most probable tube observed here is qualitatively similar to barrier-crossing instantons for double well systems with constant

diffusivity [15, 28], i.e. to the instanton which follows from the OM Lagrangian Eq. (11).

For the Stratonovich scenario the most probable tube is obtained by minimizing the integrated exit rate Eq. (34) as a functional of φ . We show the resulting most probable reference path φ^* in Fig. 4, and observe that it is almost identical to the result for constant free-diffusion exit rate. This is consistent with the facts that in the Stratonovich scenario the free-diffusion exit rate is also independent of the path, c.f. Eq. (34), and that the R^0 -order terms for both scenarios 2 and 3 yielded similar results also in the previous subsection, see Fig. 3.

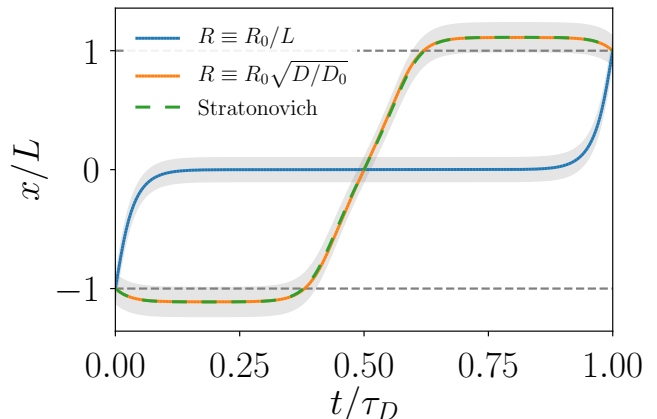


Figure 4. Most probable tubes for the three scenarios considered in Sect. III, with force and diffusivity given by Eqs. (24), (25). We minimize Eq. (14) using the same algorithm as used for functional minimization in Ref. [28]. More explicitly, we approximate the path in Eq. (14) by a finite number of 40 Fourier modes, and solve the resulting finite-dimensional minimization problem for the Fourier coefficients using a standard algorithm [44]; see Ref. [28] for more details. For the blue and orange solid lines, the minimization is carried out using the exit rate Eq. (7) to order R^0 , with a constant tube radius $R_0/L = 0.1$ (blue solid line) and a path-dependent tube radius $R(t) \equiv R_0 \sqrt{D(\varphi(t))/D_0}$ where $R_0/L = 0.1$ (orange solid line); both tubes are indicated as gray shaded area. For the blue dashed line, the integral over the exit rate Eq. (34) is minimized using $R_0/L = 0.1$. Initial and final position of the paths are shown as horizontal dashed lines.

To close this section, we now give an example for the radius dependence of the most probable tube Eq. (14). We consider a tube of constant radius $R \equiv R_0 = \text{const.}$ for the example system Eqs. (24), (25), and, as in Fig. 4, consider paths that move from $x = -L$ to $x = L$ during a time $t_f = \tau_D$. We minimize Eq. (14), evaluated using Eq. (7) to order R^2 , for each of the constant-radius tubes $R_0/L = 0.1, 0.2, 0.3$, and show the resulting most probable reference paths in Fig. 5. For $R_0/L = 0.1$ we obtain the same path φ^* as shown in Fig. 4. As discussed earlier in this section, this path remains on the barrier top for most of the transition time because the exit rate is for small radius dominated by the free-diffusion contribution Eq. (27). While for $R_0/L = 0.2$ the most probable refer-

ence path φ^* also rests at the barrier top for most of the transition time, it stays there for less time as compared to the $R_0/L = 0.1$ result; this indicates that for $R_0/L = 0.2$ the free-diffusion exit rate is already less dominant. For

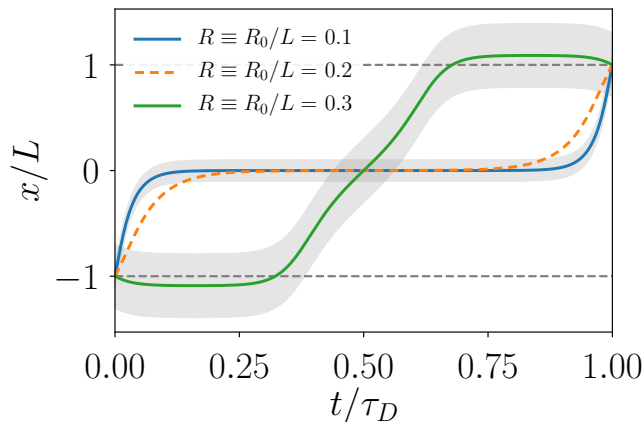


Figure 5. Most probable reference path for several constant-radius tubes. We minimize Eq. (14) using the same algorithm as describes in the caption of Fig. 4. The minimization is carried out using the exit rate Eq. (7) to order R^2 , with force and diffusivity given by Eqs. (24), (25). We show the resulting most probable reference path φ^* for a constant tube radius $R_0/L = 0.1$ (blue solid line), $R_0/L = 0.2$ (orange dashed line), and $R_0/L = 0.3$ (green solid line). For the smallest and largest tube radius, we indicate the tube as gray shaded area. Initial and final position of the paths are shown as horizontal dashed lines.

$R_0/L = 0.3$, the path φ^* is completely different from its smaller-radius counterparts. Now, the most probable reference path rests close to the well minima for most of the transition time, and crosses the barrier without stopping at the barrier top. The behavior of φ^* is now more reminiscent of the most probable tube for the constant free-diffusion exit rate scenario from Fig. 4. The reason for this is that for $R_0/L = 0.3$, the exit rate is no longer dominated by the free diffusion term Eq. (27); the next-order correction Eq. (28) is now of comparable size, as is confirmed by a simple scaling argument. By comparing the first two terms in Eq. (7), which for $N = 1$ and constant radius are given by Eqs. (27), (28), the crossover radius R_c where the exit rate is no longer dominated by the free-diffusion contribution is found as $D_0\pi^2/(4R_c^2) \approx \mathcal{L}_0$, where \mathcal{L}_0 is the typical scale of $\mathcal{L}_1^{\varphi,(0)}$. According to Fig. 3 (c), we have $\mathcal{L}_0 \approx 10\tau_D = 10L^2/D_0$, so that $(R_c/L)^2 \approx \pi^2/40 \approx 0.25$. This estimate for the crossover radius is precisely between the two radii where we observe free-diffusion dominated ($R_0/L = 0.2$) and $\mathcal{L}_1^{\varphi,(0)}$ -dominated ($R_0/L = 0.3$) most probable tube centers in Fig. 5.

This example shows that the most probable pathway for a transition can depend significantly the tube radius, i.e. on how much deviation from the reference path one tolerates.

IV. CONCLUSIONS

In this work we present a general theory for the sojourn probability, which is the probability for a diffusive trajectory to remain within a tube of small but finite time-dependent radius $R(t)$ around a continuous reference path $\varphi(t)$. For N -dimensional Langevin dynamics with multiplicative noise, using the standard Euclidean norm to define the tube, and assuming a twice continuously differentiable reference path, we derive an expansion in powers of the tube radius for the instantaneous exit rate at which stochastic trajectories first leave a small-but-finite radius tube. Based on this exit rate, we discuss the vanishing-radius limit for ratios of sojourn probabilities for pairs of reference paths, and in particular for a pair of forward and reverse path. For the special case of a one-dimensional system, $N = 1$, we derive explicit formulas for the exit rate in terms of the drift and diffusivity, and in an example consider several choices for the time-dependent tube radius. The Lagrangian Eq. (22) we derive for one-dimensional Langevin dynamics is different from the Lagrangians in the literature, and has the advantage of being directly related to an observable exit rate. We validate our perturbative theoretical results by comparing to numerical simulations of the FP dynamics. For our one-dimensional example system, we also illustrate how the most probable tube depends on both the choice of time-dependence of the tube radius, as well as the size of the tube. Our results have several important consequences, from both a mathematical and physical point of view.

The exit rate we derive is for small radius dominated by a free-diffusion contribution, consistent with the fact that Langevin dynamics is on small length- and time scales dominated by the noise term, as compared to the drift term [39]. For additive noise, the dominating free-diffusion contribution to the exit rate is independent of the reference path, so that limiting ratios of sojourn probabilities for constant-radius tubes probe subleading-order terms of the exit rate, and can be used to define the stochastic action [3–9, 27]. For state-dependent noise, the local free-diffusion exit rate is also state-dependent, and the ratio of sojourn probabilities for two constant-radius tubes is in general either zero or infinity in the limit of vanishing tube radius; this means that one path is typically infinitely more likely than the other. Our theory thus provides an intuitive picture as to why classical definitions of stochastic actions for additive-noise systems cannot be simply generalized to systems with multiplicative noise [4].

Our work elucidates the geometry behind mathematical attempts to obtain a finite limiting-ratio for pairs of sojourn probabilities [3, 5, 8, 9]. These works do not consider the sojourn probability to remain within a moving ball (defined with respect to the standard Euclidean norm) centered at a reference path, but instead the sojourn probability to remain within more complicated geometrical shapes, which are not necessarily centered at the

reference path. Because these definitions of the tubular neighborhood use the diffusion tensor of the underlying stochastic dynamics, this tensor needs to be known to measure such finite-radius sojourn probabilities in an experiment. More so, from an experimental point of view it is more natural to simply consider a constant-radius tube with respect to the metric of the ambient Euclidean space. The corresponding sojourn probability is, for one-dimensional systems, quantified by our explicit results Eqs. (27), (28).

While limiting ratios of sojourn probabilities for arbitrary pairs of paths do not lead to finite results, a pair consisting of forward and reverse path does. This implies that limits of sojourn probabilities can be used to quantify irreversibility along individual paths, and indeed for $N = 1$ our results recover established formulas for the path-wise entropy production [25, 33, 38].

Besides discussing the technical difficulties and ambiguities arising from trying to define vanishing-radius limits of sojourn probabilities for systems with multiplicative noise, our work focuses on considering finite-radius tubes. From a mathematical perspective, instead of trying to introduce a probability *density* on the space of all continuous functions, we evaluate the probability *measure* induced on that space by Langevin dynamics. Because of this there is no need to consider any limiting procedures in our theory, and indeed it has been shown that for Langevin dynamics with multiplicative noise a probability density on the space of all continuous paths does not even exist [4].

From a physical point of view, considering the finite-radius tubular ensemble also makes sense. The probability to observe a given individual stochastic trajectory vanishes, so that it is not straightforward to quantify it in an experiment. The probability to observe any stochastic trajectory of the finite-radius tubular ensemble is positive, and hence is directly accessible in experiment, simply by counting how many stochastic trajectories that started within the tube remain until a later time [27]. Finite-radius tubes can thus be used to probe path-properties in experiment and simulation, and indeed for additive noise they have been used to infer both ratios of path probabilities [28] and the entropy production along individual paths [38].

Our results demonstrate that the most probable tube depends sensitively on both the protocol for the time-dependence of the tube radius, and on the size of the tube. Thus, because in practice there is typically a finite amount of deviation from a reference path one is willing to tolerate, considering the single most probable path in general does not yield physically relevant results. The concept of the most probable tube will be useful for understanding in more depth the properties of transition paths [17, 18, 22], for example by investigating how a small time-dependent tube radius can be chosen so as to capture as many transition paths as possible.

Another interesting direction for future research is considering the ratio of sojourn probabilities for for-

ward/reverse path pairs also at finite tube radius, and relate the resulting expression to the path integral of the path-wise entropy production over all stochastic trajectories in the corresponding tubular ensemble. This will yield a generalization of the path-wise entropy production [24–26, 38] to tubes.

To date, for multiplicative noise and dimension $N \geq 2$, no explicit representation in terms of \mathbf{a} , \mathbf{D} is available for the exit rate Eq. (7) from a tube with small-but-finite constant radius (defined via the standard Euclidean metric). Since this exit rate is arguably the most straightforward experimental observable to quantify the probability of a given pathway, an important next step will be calculating explicit expressions for the exit rate, in terms of \mathbf{a} , \mathbf{D} , also for dimensions larger than $N = 1$. From our results for one-dimensional systems, it is expected that the R^0 contribution to the resulting exit rate will be different from the Stratonovich Lagrangian [3].

In summary, our theory on sojourn probabilities for diffusive stochastic dynamics provides a comprehensive and physical picture of the rather technical literature on path probabilities for systems with state-dependent noise, relates the concept of path probabilities to measurement, and in particular for the first time quantifies the probability for a stochastic trajectory to remain within a constant-radius tube around a twice continuously differentiable reference path.

ACKNOWLEDGMENTS

Work was funded in part by the European Research Council under the EU’s Horizon 2020 Program, Grant No. 740269, and by an Early Career Grant to RA from the Isaac Newton Trust.

Appendix A: Exit rate for the N -dimensional FPE in terms of instantaneous spectrum

In the present appendix, we derive the expression Eq. (7) for the exit rate from a tube with time-dependent radius $R(t)$ around a path $\varphi(t)$ for the Langevin dynamics. The present derivation is a generalization of a calculation from Ref. [27] for the exit rate for Langevin dynamics with additive noise and a noise matrix proportional to the unit matrix; we will only highlight the differences to this previous derivation, and refer the reader to Ref. [27] for more details. Throughout this appendix, we assume that φ is twice continuously differentiable, and use the standard Euclidean norm $\|\mathbf{x}\|_2 \equiv \sqrt{x_1^2 + x_2^2 + \dots + x_N^2}$ to define the tube around φ .

1. FPE in dimensionless streaming coordinates

To eliminate the time-dependence of the spatial domain Eq. (16), we introduce the dimensionless streaming

variables

$$\tilde{t}(t) \equiv \frac{t}{\tau_D}, \quad \tilde{\mathbf{x}}(\mathbf{x}, t) \equiv \frac{\mathbf{x} - \boldsymbol{\varphi}(t)}{R(t)}, \quad (\text{A1})$$

where $\tau_D \equiv L^2/D_0$ is the time scale on which a particle diffuses over the typical length scale L of the external force \mathbf{a} with a typical diffusive scale D_0 . The domain for $\tilde{\mathbf{x}}$ is then independent of time and given by the unit ball,

$$\tilde{\mathbf{x}} \in \tilde{B} \equiv \{ \tilde{\mathbf{x}} \mid \|\tilde{\mathbf{x}}\|_2 < 1 \}. \quad (\text{A2})$$

We furthermore define a dimensionless probability density $\tilde{P}_\epsilon^\varphi$, a dimensionless drift $\tilde{\mathbf{a}}$ and diffusion tensor $\tilde{\mathbf{D}}$, and a dimensionless path $\tilde{\varphi}$ as $\tilde{P}_\epsilon^\varphi(\tilde{\mathbf{x}}, \tilde{t}) \equiv R(t)^N P_R^\varphi(\mathbf{x}, t)$, $\tilde{\mathbf{a}}(\tilde{\mathbf{x}}, \tilde{t}) \equiv \tau_D \mathbf{a}(\mathbf{x}, t)/L$, $\tilde{\mathbf{D}}(\tilde{\mathbf{x}}, \tilde{t}) \equiv \mathbf{D}(\mathbf{x}, t)/D_0$, $\tilde{\varphi}(\tilde{t}) \equiv \boldsymbol{\varphi}(t)/L$, where (\mathbf{x}, t) and $(\tilde{\mathbf{x}}, \tilde{t})$ are related as defined in Eq. (A1). Here and below, dimensionless quantities are always indicated by a tilde. In dimensionless form the FPE, Eq. (15), becomes

$$\tilde{\epsilon}^2 \partial_{\tilde{t}} \tilde{P}_\epsilon^\varphi = \tilde{\mathcal{F}}_{\text{app}} \tilde{P}_\epsilon^\varphi, \quad (\text{A3})$$

with the dimensionless time-dependent tube radius

$$\tilde{\epsilon}(\tilde{t}) \equiv \frac{R(\tilde{t})}{L}, \quad (\text{A4})$$

and the dimensionless apparent Fokker-Planck (FP) operator $\tilde{\mathcal{F}}_{\text{app}}$, given by

$$\tilde{\mathcal{F}}_{\text{app}} \tilde{P}_\epsilon^\varphi \equiv -\tilde{\epsilon} \tilde{\nabla}_i (\tilde{a}_{\text{app},i} \tilde{P}_\epsilon) + \tilde{\nabla}_i \tilde{\nabla}_j (\tilde{D}_{ij} \tilde{P}_\epsilon) \quad (\text{A5})$$

the derivative with respect to $\tilde{\mathbf{x}}$ is given by $\tilde{\nabla}_j \equiv \partial/\partial \tilde{x}_j = R \partial/\partial x_j$, and where the apparent drift is given by

$$\tilde{\mathbf{a}}_{\text{app}} = \tilde{\mathbf{a}} - \dot{\tilde{\varphi}} - \dot{\tilde{\epsilon}} \tilde{\mathbf{x}}. \quad (\text{A6})$$

A dot over a function in dimensionless (dimensional) form always signifies a derivative with respect to dimensionless (dimensional) time. For example, $\dot{\tilde{\varphi}} = L/\tau_D \dot{\boldsymbol{\varphi}}$ and $\dot{R}/L = \dot{\epsilon}/\tau_D$. Dots are used interchangeably with the symbols ∂_t , $\partial_{\tilde{t}}$. As can be seen directly from Eq. (A6), with respect to the coordinate system $(\tilde{\mathbf{x}}, \tilde{t})$, the velocity of the path $\boldsymbol{\varphi}$ acts as a fictitious spatially constant drift inside the tube, and the change in tube radius leads to a fictitious linear drift. Since these are apparent drift terms, which are due to our choice of coordinate system, we call $\tilde{\mathbf{a}}_{\text{app}}$ the apparent drift and $\tilde{\mathcal{F}}_{\text{app}}$ the apparent FP operator.

In dimensionless streaming coordinates, the time-dependent absorbing boundary condition at $\tilde{\mathbf{x}} \in \partial B_R^\varphi(t)$ becomes

$$\tilde{P}_\epsilon^\varphi(\tilde{\mathbf{x}}, \tilde{t}) = 0 \quad \forall \|\tilde{\mathbf{x}}\|_2 = 1, \quad (\text{A7})$$

which is independent of time. This is the principal advantage of using streaming coordinates.

2. Approximate solution of the FPE

We expand the probability distribution $\tilde{P}_\epsilon^\varphi$ in Eq. (A3) in terms of the instantaneous FP eigenstates $\tilde{\rho}_n(\tilde{\mathbf{x}}, \tilde{t})$ as

$$\tilde{P}_\epsilon^\varphi(\tilde{\mathbf{x}}, \tilde{t}) = \sum_{m=1}^{\infty} \tilde{a}_m(\tilde{t}) \tilde{\rho}_m(\tilde{\mathbf{x}}, \tilde{t}). \quad (\text{A8})$$

At time \tilde{t} the eigenvalues $-\tilde{\lambda}_n(\tilde{t})$ and eigenfunctions $\tilde{\rho}_n(\tilde{\mathbf{x}}, \tilde{t})$ of the apparent dimensionless FP operator $\tilde{\mathcal{F}}_{\text{app}}(\tilde{t})$ fulfill the eigenvalue equation

$$\tilde{\mathcal{F}}_{\text{app}}(\tilde{t}) \tilde{\rho}_n(\tilde{\mathbf{x}}, \tilde{t}) = -\tilde{\lambda}_n(\tilde{t}) \tilde{\rho}_n(\tilde{\mathbf{x}}, \tilde{t}) \quad (\text{A9})$$

and the absorbing boundary conditions $\tilde{\rho}_n(\tilde{\mathbf{x}}, \tilde{t}) = 0$ for $\|\tilde{\mathbf{x}}\|_2 = 1$. We assume the eigenvalues to be ordered, i.e. $\tilde{\lambda}_n \leq \tilde{\lambda}_m$ for $n < m$, and due to the absorbing boundary condition we have $\tilde{\lambda}_1 > 0$. We assume that at any time \tilde{t} there exists an instantaneous steady-state solution $\tilde{\rho}_{\text{ss}}(\tilde{\mathbf{x}}, \tilde{t})$ of Eq. (A3) with reflecting boundary conditions at $\|\tilde{\mathbf{x}}\|_2 = 1$. We do not require $\tilde{\rho}_{\text{ss}}$ to be normalized, and in App. B discuss a perturbative approach to calculating $\tilde{\rho}_{\text{ss}}$ as a power series in $\tilde{\epsilon}$. Using the instantaneous steady-state $\tilde{\rho}_{\text{ss}}$ we introduce the instantaneous inner product

$$\langle f, g \rangle \equiv \int_{\tilde{B}} d^N \tilde{\mathbf{x}} f(\tilde{\mathbf{x}}) g(\tilde{\mathbf{x}}) / \tilde{\rho}_{\text{ss}}(\tilde{\mathbf{x}}, \tilde{t}). \quad (\text{A10})$$

With respect to this inner product, the FP operator $\tilde{\mathcal{F}}_{\text{app}}$ is self-adjoint so that the absorbing-boundary eigenfunctions $\tilde{\rho}_n$ can be chosen orthogonal at each time \tilde{t} [39].

Expanding the probability distribution $\tilde{P}_\epsilon^\varphi$ in Eq. (A3) in terms of the instantaneous FP eigenstates, as given by Eq. (A8), and projecting the equation onto $\tilde{\rho}_n$ using the inner product Eq. (A10), yields

$$-\dot{\tilde{a}}_n = \frac{\tilde{\lambda}_n}{\tilde{\epsilon}^2} \tilde{a}_n + \sum_{m=1}^{\infty} \frac{\langle \dot{\tilde{\rho}}_n, \dot{\tilde{\rho}}_m \rangle}{\langle \tilde{\rho}_n, \tilde{\rho}_n \rangle} \tilde{a}_m, \quad (\text{A11})$$

where $n \in \mathbb{N}$ and a dot here denotes a derivative with respect to \tilde{t} . Because the apparent FP operator is time-dependent, both the eigenvalues $\tilde{\lambda}_n$ and the inner products $\langle \dot{\tilde{\rho}}_n, \dot{\tilde{\rho}}_m \rangle$, $\langle \tilde{\rho}_n, \tilde{\rho}_n \rangle$, are functions of \tilde{t} . The FPE, Eq. (15), with absorbing boundary conditions is equivalent to Eq. (A11); once the latter is solved, the dimensionless probability density inside the tube is obtained from Eq. (A8), which can be recast in physical units using the definitions of the dimensionless quantities given in Sect. A 1.

Since $\tilde{\mathcal{F}}_{\text{app}}$ depends on $\tilde{\epsilon}$, so do $\tilde{\lambda}_n$, $\langle \dot{\tilde{\rho}}_n, \dot{\tilde{\rho}}_m \rangle$, $\langle \tilde{\rho}_n, \tilde{\rho}_n \rangle$, which appear in Eq. (A11). From Eq. (A5) it is apparent that the ratio of the off-diagonal to diagonal terms in Eq. (A11) is at least of order $\tilde{\epsilon}^2$. Thus, mode-coupling effects are sub-dominant and the uncoupled dynamics provides a good first approximation for small $\tilde{\epsilon}$. In the context of time-dependent perturbation theory in quantum mechanics, this is known as the adiabatic approximation [41].

While Eq. (A11) looks identical to the corresponding equation in Ref. [27], there are two important differences. First, in the present work we consider a time-dependent $\tilde{\epsilon}$, whereas in Ref. [27] the tube radius was assumed constant. Second, because of the state-dependent noise matrix in Eq. (A5), the spectrum of the FPE in general depends on \tilde{t} also to lowest order in $\tilde{\epsilon}$; by contrast, in

Ref. [27], the spectrum was to lowest order independent of \tilde{t} . Thus, while in this previous work mode-coupling effects were only relevant at order $\tilde{\epsilon}^3$, in the present work they can become relevant already at order $\tilde{\epsilon}^2$. Taking these two differences into account, the derivation of an approximate propagator for Eq. (A11) carried out in Ref. [27] is straightforwardly applied also in the present scenario, and leads to

$$\begin{aligned} \tilde{P}_\epsilon^\varphi(\tilde{\mathbf{x}}, \tilde{t} \mid \tilde{\mathbf{x}}_i, \tilde{t}_i) &= \exp \left[- \int_{\tilde{t}_i}^{\tilde{t}} d\tilde{t}' \frac{\tilde{\Lambda}_1(\tilde{t}')}{\tilde{\epsilon}^2(\tilde{t}')} \right] \frac{1}{\tilde{\rho}_{\text{ss}}(\tilde{\mathbf{x}}_i, \tilde{t}_i) \langle \tilde{\rho}_1, \tilde{\rho}_1 \rangle_{\tilde{t}_i}} \\ &\times \left[\tilde{\rho}_1(\tilde{\mathbf{x}}, \tilde{t}) - \sum_{m=2}^{\infty} \frac{\tilde{\epsilon}^2(\tilde{t})}{\Delta \tilde{\Lambda}_{m1}(\tilde{t})} \frac{\langle \tilde{\rho}_m, \dot{\tilde{\rho}}_1 \rangle}{\langle \tilde{\rho}_m, \tilde{\rho}_m \rangle} \Big|_{\tilde{t}} \tilde{\rho}_m(\tilde{\mathbf{x}}, \tilde{t}) \right] \left[\tilde{\rho}_1(\tilde{\mathbf{x}}_i, \tilde{t}_i) - \sum_{m=2}^{\infty} \frac{\tilde{\epsilon}^2(\tilde{t}_i)}{\Delta \tilde{\Lambda}_{m1}(\tilde{t}_i)} \frac{\langle \tilde{\rho}_1, \dot{\tilde{\rho}}_m \rangle}{\langle \tilde{\rho}_m, \tilde{\rho}_m \rangle} \Big|_{\tilde{t}_i} \tilde{\rho}_m(\tilde{\mathbf{x}}_i, \tilde{t}_i) \right] \\ &+ \mathcal{O}(\tilde{\epsilon}^4), \end{aligned} \quad (\text{A12})$$

where

$$\tilde{\Lambda}_n \equiv \tilde{\lambda}_n + \tilde{\epsilon}^2 \frac{\langle \tilde{\rho}_n, \dot{\tilde{\rho}}_n \rangle}{\langle \tilde{\rho}_n, \tilde{\rho}_n \rangle}, \quad (\text{A13})$$

$$\Delta \tilde{\Lambda}_{mn} \equiv \tilde{\Lambda}_m - \tilde{\Lambda}_n. \quad (\text{A14})$$

The approximate FP propagator Eq. (A12) and valid after an initial decay time $\tilde{\tau}_{\text{rel}}$ given by

$$\tilde{t} - \tilde{t}_i \gtrsim \tilde{\tau}_{\text{rel}} \equiv \frac{\tilde{\epsilon}^2}{\Delta \Lambda_{21}}, \quad (\text{A15})$$

and neglects terms that are exponentially small as compared to the terms present in Eq. (A12). In contrast to its counterpart in Ref. [27], the propagator Eq. (A12) i) features a time-dependent $\tilde{\epsilon}$, and ii) is valid only to order $\tilde{\epsilon}^3$.

Using Eq. (A12), we can express the solution for an arbitrary initial distribution \tilde{P}_i inside the tube as

$$\tilde{P}_\epsilon^\varphi(\tilde{\mathbf{x}}, \tilde{t} \mid \tilde{\mathbf{X}}_{\tilde{t}_i} \sim \tilde{P}_i) = \int_{\tilde{B}} d^N \tilde{\mathbf{x}}_i \tilde{P}_\epsilon^\varphi(\tilde{\mathbf{x}}, \tilde{t} \mid \tilde{\mathbf{x}}_i, \tilde{t}_i) \tilde{P}_i(\tilde{\mathbf{x}}_i), \quad (\text{A16})$$

from which the survival probability, Eq. (17), follows in dimensionless form as

$$\tilde{P}_\epsilon^\varphi(\tilde{t} \mid \tilde{\mathbf{X}}_{\tilde{t}_i} \sim \tilde{P}_i) = \int_{\tilde{B}} d^N \tilde{\mathbf{x}} \tilde{P}_\epsilon^\varphi(\tilde{\mathbf{x}}, \tilde{t} \mid \tilde{\mathbf{X}}_{\tilde{t}_i} \sim \tilde{P}_i). \quad (\text{A17})$$

3. Exit rate

For a particle starting at time t_i according to a distribution $\mathbf{X}_{t_i} \sim P_i$ inside the tube, the instantaneous exit rate is given by Eq. (18). Using the dimensionless quantities defined in Sect. A 1, the dimensionless instantaneous exit rate is given as

$$\tilde{\alpha}_\epsilon^\varphi(\tilde{t}) \equiv \tau_D \alpha_{\tilde{R}}^\varphi(t) = - \frac{\dot{\tilde{P}}_\epsilon^\varphi(\tilde{t})}{\tilde{P}_\epsilon^\varphi(\tilde{t})}, \quad (\text{A18})$$

where the dot denotes a derivative with respect to \tilde{t} , and $\tilde{P}_\epsilon^\varphi(\tilde{t}) \equiv \tilde{P}_\epsilon^\varphi(\tilde{t} \mid \tilde{\mathbf{X}}_{\tilde{t}_i} \sim \tilde{P}_i)$ is the survival probability in dimensionless form, with $\tilde{P}_i(\tilde{\mathbf{x}}) = R(t_i)^N P_i(\mathbf{x})$. Using the steady-state FP solution Eqs. (A12-A17), the exit rate Eq. (A18) is evaluated to yield

$$\tilde{\alpha}_\epsilon^\varphi = \frac{\tilde{\lambda}_1}{\tilde{\epsilon}^2} + \frac{\langle \tilde{\rho}_1, \dot{\tilde{\rho}}_1 \rangle}{\langle \tilde{\rho}_1, \tilde{\rho}_1 \rangle} - \frac{\partial_{\tilde{t}} (\tilde{\mathcal{I}}_1 - \tilde{\epsilon}^2 \tilde{\mathcal{S}})}{\tilde{\mathcal{I}}_1 - \tilde{\epsilon}^2 \tilde{\mathcal{S}}} + \mathcal{O}(\tilde{\epsilon}^4), \quad (\text{A19})$$

with

$$\tilde{\mathcal{I}}_n(\tilde{t}) \equiv \int_{\tilde{B}} d^N \tilde{\mathbf{x}} \tilde{\rho}_n(\tilde{\mathbf{x}}, \tilde{t}), \quad (\text{A20})$$

$$\tilde{\mathcal{S}}(\tilde{t}) \equiv \sum_{m=2}^{\infty} \frac{1}{\Delta \tilde{\Lambda}_{m1}(\tilde{t})} \frac{\langle \tilde{\rho}_m, \dot{\tilde{\rho}}_1 \rangle}{\langle \tilde{\rho}_m, \tilde{\rho}_m \rangle} \Big|_{\tilde{t}} \tilde{\mathcal{I}}_m(\tilde{t}). \quad (\text{A21})$$

Equation (A19), which is valid after the initial transient decay time $\tilde{\tau}_{\text{rel}}$ defined in Eq. (A15), is independent of the initial distribution \tilde{P}_i ; this is because in Eq. (A12) the initial condition only contributes an overall prefactor independent of $(\tilde{\mathbf{x}}, \tilde{t})$, which does not affect the relative change of particles inside the tube quantified by Eq. (A18). With Eq. (A19) the instantaneous exit rate is expressed solely in terms of the instantaneous FP spectrum inside the tube. Expanding the quantities that appear in Eq. (A19) in powers of $\tilde{\epsilon}$, and using the symmetry properties of these quantities, c.f. App. B, a power series expansion of the exit rate is obtained as

$$\tilde{\alpha}_\epsilon^\varphi = \frac{\tilde{\lambda}_1^{(0)}}{\tilde{\epsilon}^2} + \tilde{\alpha}^{\varphi,(0)} + \tilde{\epsilon}^2 \tilde{\alpha}^{\varphi,(2)} + \mathcal{O}(\tilde{\epsilon}^4), \quad (\text{A22})$$

where

$$\tilde{\alpha}_{\text{free}}^{\varphi} = \frac{\tilde{\lambda}_1^{(0)}}{\tilde{\epsilon}^2}, \quad (\text{A23})$$

$$\tilde{\alpha}^{\varphi, (0)} = \tilde{\lambda}_1^{(2)} + \frac{\langle \tilde{\rho}_1, \dot{\tilde{\rho}}_1 \rangle^{(0)}}{\langle \tilde{\rho}_1, \tilde{\rho}_1 \rangle^{(0)}} - \frac{\dot{\tilde{\mathcal{I}}}_1^{(0)}}{\tilde{\mathcal{I}}_1^{(0)}} \quad (\text{A24})$$

$$\begin{aligned} \tilde{\alpha}^{\varphi, (2)} = & \tilde{\lambda}_1^{(4)} + \frac{\langle \tilde{\rho}_1, \dot{\tilde{\rho}}_1 \rangle^{(2)}}{\langle \tilde{\rho}_1, \tilde{\rho}_1 \rangle^{(0)}} - \frac{\langle \tilde{\rho}_1, \dot{\tilde{\rho}}_1 \rangle^{(0)}}{\langle \tilde{\rho}_1, \tilde{\rho}_1 \rangle^{(0)}} \frac{\langle \tilde{\rho}_1, \tilde{\rho}_1 \rangle^{(2)}}{\langle \tilde{\rho}_1, \tilde{\rho}_1 \rangle^{(0)}} \\ & - \frac{\dot{\tilde{\mathcal{I}}}_1^{(2)} - \dot{\tilde{\mathcal{S}}}^{(0)}}{\tilde{\mathcal{I}}_1^{(0)}} - \frac{\tilde{\mathcal{I}}_1^{(2)} - \tilde{\mathcal{S}}^{(0)}}{\tilde{\mathcal{I}}_1^{(0)}} \left(2 \frac{\dot{\tilde{\epsilon}}}{\tilde{\epsilon}} - \frac{\dot{\tilde{\mathcal{I}}}_1^{(0)}}{\tilde{\mathcal{I}}_1^{(0)}} \right), \end{aligned} \quad (\text{A25})$$

with

$$\tilde{\mathcal{I}}_n^{(k)}(\tilde{t}) \equiv \int_{\tilde{B}} d^N \tilde{\mathbf{x}} \tilde{\rho}_n^{(k)}(\tilde{\mathbf{x}}, \tilde{t}), \quad (\text{A26})$$

we note again that for the perturbative calculation of the spectrum we assume that $\dot{\tilde{\epsilon}}/\tilde{\epsilon}$ scales as $\tilde{\epsilon}^0$, and by a superscript (k) we denote the k -th order contribution to a perturbation series in $\tilde{\epsilon}$, e.g.

$$\tilde{\mathcal{S}} = \sum_{k=0}^{\infty} \tilde{\epsilon}^k \tilde{\mathcal{S}}^{(k)}. \quad (\text{A27})$$

Using Eq. (A18) the exit rate in physical units, Eq. (7), is obtained from Eqs. (A22-A25); according to Eq. (A18), a scaling $\tilde{\epsilon}^k$ in $\tilde{\alpha}^{\varphi}$ (dimensionless form) translates to a scaling R^k in α_R^{φ} (physical units). According to Eq. (A5) the instantaneous FP spectrum depends on $(\varphi, \dot{\varphi}, R, \dot{R})$; because of the additional time derivatives in Eqs. (A25), (A24), the terms may additionally depend on $\ddot{\varphi}$ and \ddot{R} .

Equations (A22-A25), express the exit rate $\tilde{\alpha}^{\varphi}$ fully in terms of the perturbative spectrum of the FP operator inside the tube. If the noise is additive (i.e. independent of position) and if the tube radius is constant, $\dot{R} = 0$, then the exit rate reduces to the previous result from Ref. [27].

In App. B we derive the equations which determine the perturbation expansion of the FP spectrum, and in particular show that at time $\tilde{t} = t/\tau_D$, Eq. (A23) is the steady-state free-diffusion exit rate from a ball of radius $R(t)$ and with diffusion tensor $\underline{D}(\varphi(t), t)$. Equation (A22) thus show explicitly that for small tube radius $\tilde{\epsilon} \ll 1$, the exit from the tube is dominated by this instantaneous steady-state free-diffusion exit rate.

Appendix B: The N -dimensional FP spectrum

In the present appendix we derive the perturbative equations for the instantaneous spectrum of the dimensionless FP operator Eq. (A3) inside the tube. The present calculation generalizes a conceptually similar calculation from Ref. [27], so that we only sketch it here and refer the reader to the reference for more details.

1. Perturbation theory for the N -dimensional FP spectrum

Taylor expansion of drift and noise. The multidimensional Taylor expansion of the drift \mathbf{a} around the tube center $\varphi(t)$ is given by

$$\begin{aligned} \mathbf{a}(\mathbf{x}, t) = & \sum_{k=0}^{\infty} \frac{1}{k!} \sum_{\alpha_1, \dots, \alpha_k=1}^N \frac{\partial^k \mathbf{a}}{\partial x_{\alpha_1} \dots \partial x_{\alpha_k}} \Big|_{(\varphi(t), t)} \\ & \times (\mathbf{x} - \varphi(t))_{\alpha_1} \dots (\mathbf{x} - \varphi(t))_{\alpha_k}, \end{aligned} \quad (\text{B1})$$

where $(\mathbf{x} - \varphi(t))_{\alpha_i} \equiv x_{\alpha_i} - \varphi_{\alpha_i}(t)$ is the α_i -th component of the vector $\mathbf{x} - \varphi(t)$. Substituting this Taylor expansion into the dimensionless variables from Sect. A 1, we obtain

$$\tilde{\mathbf{a}}_{\text{app}}(\tilde{\mathbf{x}}, \tilde{t}) = - \sum_{k=1}^{\infty} \tilde{\epsilon}^{k-1} k \quad (\text{B2})$$

$$\begin{aligned} & \times \sum_{\alpha_1, \dots, \alpha_{k-1}=1}^N \tilde{\mathbf{E}}_{k, \alpha_1 \dots \alpha_{k-1}}(\tilde{t}) \tilde{x}_{\alpha_1} \dots \tilde{x}_{\alpha_{k-1}} \\ & \equiv - \sum_{k=1}^{\infty} \tilde{\epsilon}^{k-1} k \tilde{\mathbf{E}}_{k, \alpha}(\tilde{t}) \tilde{x}_{\alpha} \end{aligned} \quad (\text{B3})$$

where we use the Einstein sum convention for the indices $\alpha \equiv (\alpha_1, \dots, \alpha_{k-1})$, abbreviate $\tilde{x}_{\alpha} \equiv \tilde{x}_{\alpha_1} \dots \tilde{x}_{\alpha_{k-1}}$, and the vector-valued $(k-1)$ -multilinear form $\tilde{\mathbf{E}}_k$ is defined as

$$\begin{aligned} \tilde{\mathbf{E}}_{k, \alpha_1 \dots \alpha_{k-1}}(\tilde{t}) \equiv & - \frac{1}{k!} L^{k-1} \tau_D \frac{\partial^{k-1} \mathbf{a}}{\partial x_{\alpha_1} \dots \partial x_{\alpha_{k-1}}} \Big|_{(\varphi(t), t)} \\ & + \delta_{k,1} \dot{\tilde{\varphi}}(\tilde{t}) + \frac{\delta_{k,2}}{2} \frac{\dot{\tilde{\epsilon}}(\tilde{t})}{\tilde{\epsilon}(\tilde{t})} \end{aligned} \quad (\text{B4})$$

where dimensionless quantities (as indicated by a tilde) and quantities with physical dimensions are related as defined in Sect. A 1. We recall that we assume $\dot{\tilde{\epsilon}}/\tilde{\epsilon}$ scales as $\tilde{\epsilon}^0$.

Similarly to $\tilde{\mathbf{a}}$, by Taylor expansion of the diffusion tensor elements D_{ij} around the tube center $\varphi(t)$ we obtain an expansion

$$\tilde{D}_{ij}(\tilde{\mathbf{x}}, \tilde{t}) = \sum_{k=0}^{\infty} \tilde{\epsilon}^k \tilde{\mathcal{D}}_{ij, \alpha_1 \dots \alpha_k}^{(k)} \tilde{x}_{\alpha_1} \dots \tilde{x}_{\alpha_k}, \quad (\text{B5})$$

where

$$\tilde{\mathcal{D}}_{ij, \alpha_1 \dots \alpha_k}^{(k)}(\tilde{t}) \equiv \frac{L^k}{k! D_0} \frac{\partial^k D_{ij}}{\partial x_{\alpha_1} \dots \partial x_{\alpha_k}} \Big|_{(\varphi(t), t)}. \quad (\text{B6})$$

Hierarchy of equations for the spectrum. Inserting the power series Eqs. (B3), (B5), into the eigenvalue Eq. (A9), expanding both the instantaneous eigenvalues and eigenfunctions as power series in $\tilde{\epsilon}$,

$$\tilde{\lambda}_n = \sum_{k=0}^{\infty} \tilde{\epsilon}^k \tilde{\lambda}_n^{(k)}, \quad \tilde{\rho}_n = \sum_{k=0}^{\infty} \tilde{\epsilon}^k \tilde{\rho}_n^{(k)}, \quad (\text{B7})$$

and demanding that the resulting equation hold at each power $\tilde{\epsilon}^k$, we obtain a hierarchy of equations for the spectrum. For the n -th eigenvalue/eigenfunction pair at order $\tilde{\epsilon}^k$, this yields

$$\begin{aligned} \tilde{\mathcal{D}}_{ij}^{(0)} \tilde{\nabla}_i \tilde{\nabla}_j \tilde{\rho}_n^{(k)} + \tilde{\lambda}_n^{(0)} \tilde{\rho}_n^{(k)} &= - \sum_{l=1}^k \tilde{\lambda}_n^{(l)} \tilde{\rho}_n^{(k-l)} \\ - \sum_{l=1}^k l \tilde{E}_{l,\alpha}^i \tilde{\nabla}_i \left(\tilde{x}_\alpha \tilde{\rho}_n^{(k-l)} \right) &- \sum_{\substack{m \geq 0 \\ l \geq 1 \\ l+m=k}} \tilde{\mathcal{D}}_{ij,\alpha}^{(l)} \tilde{\nabla}_i \tilde{\nabla}_j \left[\tilde{x}_\alpha \tilde{\rho}_n^{(m)} \right] \end{aligned} \quad (\text{B8})$$

where we use the convention that for $k = 0$, the sums on the right-hand side are zero. For the absorbing boundary conditions to be fulfilled independently of $\tilde{\epsilon}$, they need to hold at each order separately, so that for all $k \in \{0, 1, 2, \dots\}$ we have

$$\tilde{\rho}_n^{(k)}(\tilde{\mathbf{x}}, \tilde{t}) = 0 \quad \forall \tilde{\mathbf{x}} \in \partial \tilde{B} \equiv \{ \tilde{\mathbf{x}} \mid \|\tilde{\mathbf{x}}\|_2 = 1 \}. \quad (\text{B9})$$

While any solution to Eqs. (B8), (B9) can be used in practice for the spectrum, the solution to these equations is not unique. To fix the solution uniquely, we introduce a normalization condition $\langle \tilde{\rho}_n, \tilde{\rho}_n \rangle = 1$, where the inner product is defined in Eq. (A10). Inserting the power series expansion Eq. (B7) for the eigenfunction into this normalization condition, and demanding that the condition hold at each power of $\tilde{\epsilon}$, we obtain for $k = 0$ that

$$\int_{\tilde{B}} d^N \tilde{\mathbf{x}} \tilde{\rho}_n^{(0)} \tilde{\rho}_n^{(0)} = 1, \quad (\text{B10})$$

while for $k \geq 1$ we have that

$$\begin{aligned} \int_{\tilde{B}} d^N \tilde{\mathbf{x}} \tilde{\rho}_n^{(k)} \tilde{\rho}_n^{(0)} \\ = - \frac{1}{2} \sum_{l=0}^{k-1} \sum_{m=0}^{k-\max\{1,l\}} \int_{\tilde{B}} d^N \tilde{\mathbf{x}} \tilde{\rho}_n^{(l)} \tilde{\rho}_n^{(m)} (\tilde{\rho}_{\text{ss}}^{-1})^{(k-l-m)}, \end{aligned} \quad (\text{B11})$$

where we use the convention that for $k = 1$ the sum on the right-hand side is zero and the expansion of $\tilde{\rho}_{\text{ss}}^{-1}$ in powers of $\tilde{\epsilon}$ is discussed in App. B2. Note that for any k , only perturbation terms $\tilde{\rho}_n^{(l)}$ with $l < k$ appear on the right-hand side of Eq. (B11).

Equations (B8), (B9), (B10), (B11), constitute a closed system of equations that can be solved recursively to obtain the spectrum to arbitrary order.

At order $k = 0$, the right-hand side of Eq. (B8) vanishes, so that the equation is reduced to the eigenvalue equation of the anisotropic Laplace operator,

$$\tilde{\mathcal{D}}_{ij}^{(0)} \tilde{\nabla}_i \tilde{\nabla}_j \tilde{\rho}_n^{(0)} = -\tilde{\lambda}_n^{(0)} \tilde{\rho}_n^{(0)}. \quad (\text{B12})$$

Thus, $\tilde{\lambda}_n^{(0)}, \tilde{\rho}_n^{(0)}$ is the spectrum of the anisotropic Laplace operator in a unit ball with absorbing boundary conditions, and where we assume that $\tilde{\rho}_n^{(0)}$ has been normalized according to Eq. (B10). From Eq. (B12) we see that, at

time \tilde{t} , to lowest order the spectrum is that of free diffusion with a diffusion tensor $\tilde{\mathcal{D}}_{ij}^{(0)}(\tilde{t}) \equiv D_{ij}(\boldsymbol{\varphi}(\tilde{t}), \tilde{t})/D_0$; in particular, $\tilde{\lambda}_1^{(0)}$ is the corresponding instantaneous steady-state free-diffusion exit rate. Using Eq. (A23), the definition of the function f in Eq. (8) thus follows. Note that because the diffusion matrix D_{ij} is by definition symmetric, it can be diagonalized via an eigenbasis that is orthonormal with respect to the standard Euclidean inner product. By expressing Eq. (B12) with respect to such an eigenbasis of D_{ij} , and subsequently rescaling each axis by the corresponding eigenvalue, it is seen that the equation is equivalent to the eigenvalue equation for the Laplace operator in an N -dimensional ellipsoid (and with absorbing boundary conditions).

Assuming the spectrum has been obtained up to order $k - 1$, the contribution at order k is calculated as follows [27]. An equation for $\tilde{\lambda}_n^{(k)}$ is obtained by multiplying Eq. (B8) with $\tilde{\rho}_n^{(0)}$, and subsequently integrating over $\tilde{\mathbf{x}}$. Upon integrating the result by parts and using the absorbing boundary conditions Eq. (B9), it follows that the equation is in fact independent of $\tilde{\rho}_n^{(k)}$ and can be solved directly for $\tilde{\lambda}_n^{(k)}$, leading to

$$\begin{aligned} \tilde{\lambda}_n^{(k)} &= - \sum_{l=1}^{k-1} \tilde{\lambda}_n^{(l)} \int_{\tilde{B}} d^N \tilde{\mathbf{x}} \tilde{\rho}_n^{(0)} \tilde{\rho}_n^{(k-l)} \\ &- \sum_{l=1}^k l \int_{\tilde{B}} d^N \tilde{\mathbf{x}} \tilde{\rho}_n^{(0)} \tilde{E}_{l,\alpha}^i \tilde{\nabla}_i \left(\tilde{x}_\alpha \tilde{\rho}_n^{(k-l)} \right), \\ &- \sum_{\substack{m \geq 0 \\ l \geq 1 \\ l+m=k}} \tilde{\mathcal{D}}_{ij,\alpha}^{(l)} \int_{\tilde{B}} d^N \tilde{\mathbf{x}} \left[\tilde{\rho}_n^{(0)} \tilde{\nabla}_i \tilde{\nabla}_j \left(\tilde{x}_\alpha \tilde{\rho}_n^{(m)} \right) \right] \end{aligned} \quad (\text{B13})$$

where we used the normalization condition Eq. (B10) for $\tilde{\rho}_n^{(0)}$. Since the right-hand only depends on $\tilde{\lambda}_n^{(l)}, \tilde{\rho}_n^{(l)}$ with $l < k$, this equation can be used to calculate the order k eigenvalue contribution in terms of the lower-order contributions.

Once $\tilde{\lambda}_n^{(k)}$ has been obtained via Eq. (B13), the right-hand side of Eq. (B8) is known, so that to obtain $\tilde{\rho}_n^{(k)}$ the inhomogeneous anisotropic Helmholtz Eq. (B8) with boundary conditions Eq. (B9) has to be solved. In App. C we calculate the lowest-order contributions to the spectrum for $N = 1$ explicitly. Before that we now establish some general properties of the spectrum which follow from parity symmetry, and discuss the perturbation series of $\tilde{\rho}_{\text{ss}}$.

Parity properties of the spectrum. We introduce the parity operator $\tilde{\mathcal{P}}$, defined by its action on a function f as

$$(\tilde{\mathcal{P}}f)(\tilde{\mathbf{x}}) \equiv f(-\tilde{\mathbf{x}}). \quad (\text{B14})$$

Consequently, for products of functions f, g , it holds that $\tilde{\mathcal{P}}(fg) = (\tilde{\mathcal{P}}f)(\tilde{\mathcal{P}}g)$, and for partial derivatives we have $\tilde{\mathcal{P}}\tilde{\nabla}_i = -\tilde{\nabla}_i$. The operator $\tilde{\mathcal{P}}$ therefore commutes with any two derivatives, $\tilde{\mathcal{P}}\tilde{\nabla}_i \tilde{\nabla}_j = \tilde{\nabla}_i \tilde{\nabla}_j \tilde{\mathcal{P}}$, so that we can

assume that the eigenfunctions $\tilde{\rho}_n^{(0)}$ also diagonalize $\tilde{\mathcal{P}}$, i.e.

$$\tilde{\mathcal{P}}\tilde{\rho}_n^{(0)} = p_n \tilde{\rho}_n^{(0)}, \quad (\text{B15})$$

with $p_n \in \{-1, 1\}$. As in Ref. [27], via induction in k it follows from Eqs. (B8), (B9), (B13), (B15), that

$$\tilde{\lambda}_n^{(k)} = 0 \quad \text{for } k \text{ odd}, \quad (\text{B16})$$

and furthermore that

$$\tilde{\mathcal{P}}\tilde{\rho}_n^{(k)} = (-1)^k p_n \tilde{\rho}_n^{(k)}. \quad (\text{B17})$$

Thus, $\tilde{\rho}_n^{(k)}$ has the same parity as $\tilde{\rho}_n^{(0)}$ if k is even, and the opposite parity as $\tilde{\rho}_n^{(0)}$ if k is odd.

2. Perturbation theory for the reflecting-boundary steady state

In the present section we discuss the perturbative calculation and parity properties of both the steady state $\tilde{\rho}_{\text{ss}}$ and its multiplicative inverse $\tilde{\rho}_{\text{ss}}^{-1} \equiv 1/\tilde{\rho}_{\text{ss}}$.

Perturbative calculation of $\tilde{\rho}_{\text{ss}}$. According to Eq. (A5), the instantaneous formal steady state $\tilde{\rho}_{\text{ss}}$ is the solution of the boundary value problem

$$\tilde{\nabla}_i \tilde{\mathcal{J}}_{\text{ss},i} = 0, \quad (\text{B18})$$

with boundary condition

$$\left[\hat{n}_i \tilde{\mathcal{J}}_{\text{ss},i} \right] \Big|_{\partial \tilde{B}} = 0, \quad (\text{B19})$$

where \hat{n}_i is the i -th component of the outward-pointing unit normal vector $\hat{\mathbf{n}}$ on $\partial \tilde{B}$, and where

$$\tilde{\mathcal{J}}_{\text{ss},i} = \tilde{\epsilon} \tilde{a}_{\text{app},i} \tilde{\rho}_{\text{ss}} - \tilde{\nabla}_j \left(\tilde{D}_{ij} \tilde{\rho}_{\text{ss}} \right). \quad (\text{B20})$$

Similar to the discussion of the spectrum in Sect. B 1, we now derive the determining equations for the perturbative expansion for $\tilde{\rho}_{\text{ss}}$. Substituting the power series expansion Eqs. (B3), (B5) of $\tilde{a}_{\text{app},i}$ and \tilde{b}_{ij} , into Eqs. (B18), (B20), expanding the instantaneous steady state as power series in $\tilde{\epsilon}$,

$$\tilde{\rho}_{\text{ss}} = \sum_{k=0}^{\infty} \tilde{\epsilon}^k \tilde{\rho}_{\text{ss}}^{(k)}, \quad (\text{B21})$$

and demanding that the resulting equation hold at each power $\tilde{\epsilon}^k$, we obtain from Eq. (B18) a hierarchy of equations which at order $\tilde{\epsilon}^k$ reads

$$\begin{aligned} \tilde{D}_{ij}^{(0)} \tilde{\nabla}_i \tilde{\nabla}_j \tilde{\rho}_{\text{ss}}^{(k)} &= - \sum_{l=1}^k l \tilde{E}_{l,\alpha}^i \tilde{\nabla}_i \left(\tilde{x}_\alpha \tilde{\rho}_{\text{ss}}^{(k-l)} \right) \\ &- \sum_{\substack{m \geq 0 \\ l \geq 1 \\ l+m=k}} \tilde{D}_{ij,\alpha}^{(l)} \tilde{\nabla}_i \tilde{\nabla}_j \left[\tilde{x}_\alpha \tilde{\rho}_n^{(m)} \right], \end{aligned} \quad (\text{B22})$$

where we use the convention that for $k = 0$, the sums on the right-hand side are zero. Inserting the power series expansions Eq. (B3), (B5), (B21), into the boundary condition Eq. (B19), and demanding that the resulting equation be fulfilled at each power $\tilde{\epsilon}^k$, we obtain

$$\begin{aligned} 0 &= - \sum_{l=1}^k l \tilde{E}_{l,\alpha}^i \left[\hat{n}_i \left(\tilde{x}_\alpha \tilde{\rho}_{\text{ss}}^{(k-l)} \right) \right] \Big|_{\tilde{x} \in \partial \tilde{B}} \\ &- \sum_{\substack{l,m \geq 0 \\ l+m=k}} \tilde{D}_{ij,\alpha}^{(l)} \left[\hat{n}_i \tilde{\nabla}_j \left(\tilde{x}_\alpha \tilde{\rho}_n^{(m)} \right) \right] \Big|_{\tilde{x} \in \partial \tilde{B}}, \end{aligned} \quad (\text{B23})$$

where $k \geq 0$ and we use the convention that for $k = 0$, the first sum on the right-hand side is zero.

While at order $\tilde{\epsilon}^0$, the (unnormalized) solution to Eqs. (B22), (B23) is simply given by $\tilde{\rho}_{\text{ss}}^{(0)} = 1$, for $k \geq 1$ the equations have to be solved recursively, similar to the spectrum in Sect. B 1.

Parity properties of the $\tilde{\rho}_{\text{ss}}^{(k)}$. Similar to the parity properties of the FP spectrum, via induction in k it can be shown that $\tilde{\mathcal{P}}\tilde{\rho}_{\text{ss}}^{(k)} = (-1)^k \tilde{\rho}_{\text{ss}}^{(k)}$, where the parity operator $\tilde{\mathcal{P}}$ is defined in Eq. (B14).

Perturbative calculation and parity properties of $\tilde{\rho}_{\text{ss}}^{-1}$. Substituting the power series expansion Eq. (B21) of $\tilde{\rho}_{\text{ss}}$ and the expansion

$$\tilde{\rho}_{\text{ss}}^{-1} = \sum_{k=0}^{\infty} \tilde{\epsilon}^k \left(\tilde{\rho}_{\text{ss}}^{-1} \right)^{(k)}, \quad (\text{B24})$$

into the definition of the inverse, $\tilde{\rho}_{\text{ss}} \tilde{\rho}_{\text{ss}}^{-1} = 1$, and demanding that the equation hold at any order of $\tilde{\epsilon}$, we obtain a recursive system of equations for the expansion of $\tilde{\rho}_{\text{ss}}^{-1}$ [27]. From this system of equations and the parity properties of $\tilde{\rho}_{\text{ss}}^{(k)}$ it follows that

$$\tilde{\mathcal{P}} \left[\left(\tilde{\rho}_{\text{ss}}^{-1} \right)^{(k)} \right] = (-1)^k \left(\tilde{\rho}_{\text{ss}}^{-1} \right)^{(k)} \quad (\text{B25})$$

for all k .

3. Properties of power series expansions derived from parity

In the present section we give the parity properties of perturbation series relevant for the calculation of the exit rate Eq. (A19). Similar properties are derived in Ref. [27]; in contrast to the reference, where $\tilde{\rho}_1^{(0)}$ is independent of time, for multiplicative noise $\tilde{\rho}_1^{(0)}$ can depend on time.

Integral over FP eigenfunction. The spatial integral over $\tilde{\rho}_n^{(k)}$ is denoted by $\tilde{\mathcal{I}}_n^{(k)}$ and defined by Eq. (A26). From the parity properties of $\tilde{\rho}_n^{(k)}$, Eq. (B17), it follows that

$$\tilde{\mathcal{I}}_n^{(k)} = 0 \text{ if } \begin{cases} k \text{ odd and } p_n = 1, \\ k \text{ even and } p_n = -1. \end{cases} \quad (\text{B26})$$

In particular, it follows from i) the definite parity of $\tilde{\rho}_1^{(0)}$, ii) the equivalence of Eq. (B12) to a Laplace equation in an N -dimensional ellipsoid, and iii) the fact that the lowest eigenvalue of the Laplace operator is non-negative [45], that we have

$$\tilde{\mathcal{L}}_1 = \tilde{\mathcal{L}}_1^{(0)} + \tilde{\epsilon}^2 \tilde{\mathcal{L}}_1^{(2)} + \tilde{\epsilon}^4 \tilde{\mathcal{L}}_1^{(4)} + \mathcal{O}(\tilde{\epsilon}^6). \quad (\text{B27})$$

Inner product of FP eigenfunctions. The power series expansion of the inner product $\langle \tilde{\rho}_n, \tilde{\rho}_m \rangle$ is given by

$$\langle \tilde{\rho}_n, \tilde{\rho}_m \rangle = \sum_{l=0}^{\infty} \tilde{\epsilon}^l \langle \tilde{\rho}_n, \tilde{\rho}_m \rangle^{(l)}, \quad (\text{B28})$$

where

$$\langle \tilde{\rho}_n, \tilde{\rho}_m \rangle^{(l)} = \sum_{\substack{i,j,k \geq 0 \\ i+j+k=l}} \int_{\tilde{B}} d^N \tilde{\mathbf{x}} \tilde{\rho}_n^{(i)} \tilde{\rho}_m^{(j)} (\tilde{\rho}_{ss}^{-1})^{(k)} \quad (\text{B29})$$

with the power series expansions Eq. (B7), (B24). Applying the parity operator to the integrand, it follows that

$$\langle \tilde{\rho}_n, \tilde{\rho}_m \rangle^{(l)} = 0 \text{ if } \begin{cases} l \text{ odd and } p_n p_m = 1, \\ l \text{ even and } p_n p_m = -1. \end{cases} \quad (\text{B30})$$

In particular, we have

$$\langle \tilde{\rho}_n, \tilde{\rho}_n \rangle = \langle \tilde{\rho}_n, \tilde{\rho}_n \rangle^{(0)} + \tilde{\epsilon}^2 \langle \tilde{\rho}_n, \tilde{\rho}_n \rangle^{(2)} + \tilde{\epsilon}^4 \langle \tilde{\rho}_n, \tilde{\rho}_n \rangle^{(4)} + \mathcal{O}(\tilde{\epsilon}^6) \quad (\text{B31})$$

for any n .

Inner product of FP eigenfunctions including time derivative. Because a time derivative does not change spatial parity, similar to the previous case it holds that

$$\langle \tilde{\rho}_n, \dot{\tilde{\rho}}_m \rangle^{(l)} = 0 \text{ if } \begin{cases} l \text{ odd and } p_n p_m = 1, \\ l \text{ even and } p_n p_m = -1, \end{cases} \quad (\text{B32})$$

In particular, for any n we have

$$\langle \tilde{\rho}_n, \dot{\tilde{\rho}}_n \rangle = \langle \tilde{\rho}_n, \dot{\tilde{\rho}}_n \rangle^{(0)} + \tilde{\epsilon}^2 \langle \tilde{\rho}_n, \dot{\tilde{\rho}}_n \rangle^{(2)} + \mathcal{O}(\tilde{\epsilon}^4). \quad (\text{B33})$$

Appendix C: Explicit results for one-dimensional systems

In the present section, we derive explicit results for one-dimensional systems, $N = 1$.

1. Perturbation series for the 1D FPE

For $N = 1$, the the apparent dimensionless FP operator Eq. (A5) is given by

$$\tilde{\mathcal{F}}_{\text{app}} \tilde{P}_\epsilon \equiv -\tilde{\epsilon} \partial_{\tilde{x}} \left[\tilde{a}_{\text{app}} \tilde{P}_\epsilon \right] + \partial_{\tilde{x}}^2 \left[\tilde{D} \tilde{P}_\epsilon \right] \quad (\text{C1})$$

where the dimensionless apparent drift is given by

$$\tilde{a}_{\text{app}} = \tilde{a} - \dot{\tilde{\epsilon}} \tilde{x} - \dot{\tilde{\varphi}}. \quad (\text{C2})$$

We now consider the instantaneous dimensionless eigenvalue equation Eq. (A9) with absorbing boundary conditions, $\tilde{\rho}_n(\tilde{x} = \pm 1, \tilde{t}) \equiv 0$. For $N = 1$, the power series expansion Eq. (B3) for the dimensionless apparent drift becomes

$$\tilde{a}_{\text{app}}(\tilde{x}, \tilde{t}) \equiv - \sum_{k=1}^{\infty} \tilde{\epsilon}^{k-1} k \tilde{E}_k \tilde{x}^{k-1}, \quad (\text{C3})$$

with

$$\tilde{E}_k(\tilde{t}) \equiv - \frac{L^{k-1} \tau_D}{k!} \left. \frac{\partial^{k-1} a}{\partial x^{k-1}} \right|_{(\varphi(t), t)} + \delta_{k,1} \dot{\varphi}(\tilde{t}) + \frac{\delta_{k,2}}{2} \frac{\dot{\tilde{\epsilon}}(\tilde{t})}{\tilde{\epsilon}(\tilde{t})}, \quad (\text{C4})$$

where we recall that here we assume that $\dot{\tilde{\epsilon}}/\tilde{\epsilon}$ scales as $\tilde{\epsilon}^0$. The expansion Eq. (B6) of the dimensionless diffusion coefficient, is given as

$$\tilde{D}(\tilde{x}, \tilde{t}) \equiv \sum_{k=0}^{\infty} \tilde{\epsilon}^k(\tilde{t}) \tilde{D}_k(\tilde{t}) \tilde{x}^k, \quad (\text{C5})$$

with

$$\tilde{D}_k(\tilde{t}) \equiv \tilde{D}^{(k)}(\tilde{t}) \equiv \frac{1}{k!} \frac{L^k}{D_0} \left. \frac{\partial^k D}{\partial x^k} \right|_{(\varphi(t), t)}. \quad (\text{C6})$$

For a one-dimensional system, the hierarchy of equations for $(\tilde{\lambda}_n^{(k)}, \tilde{\rho}_n^{(k)})$, given by Eq. (B8), becomes

$$\begin{aligned} \partial_{\tilde{x}}^2 \tilde{\rho}_n^{(k)} + \frac{\tilde{\lambda}_n^{(0)}}{\tilde{D}_0} \tilde{\rho}_n^{(k)} &= - \frac{1}{\tilde{D}_0} \sum_{l=1}^k \tilde{\lambda}_n^{(l)} \tilde{\rho}_n^{(k-l)} \\ &- \frac{1}{\tilde{D}_0} \sum_{l=0}^{k-1} \tilde{D}_{k-l} \partial_{\tilde{x}}^2 \left(\tilde{x}^{k-l} \tilde{\rho}_n^{(l)} \right) \\ &- \frac{1}{\tilde{D}_0} \sum_{l=1}^k l \tilde{E}_l \partial_{\tilde{x}} \left[\tilde{x}^{l-1} \tilde{\rho}_n^{(k-l)} \right], \end{aligned} \quad (\text{C7})$$

where we use the convention that for $k = 0$, the sums on the right-hand side are zero. The corresponding absorbing boundary conditions Eq. (B9) are given by $\tilde{\rho}_n^{(k)}(\tilde{x} = -1, \tilde{t}) = \tilde{\rho}_n^{(k)}(\tilde{x} = 1, \tilde{t}) = 0$. Equation (C7) generalizes Eq. (C4) of Ref. [27], to which it reduces for a system with position-independent constant diffusivity $D(x, t) \equiv D_0$.

To solve Eq. (C7) recursively, the same algorithm as used in Ref. [27] for calculating the spectrum in the constant-diffusivity scenario is applicable. For completeness, we now give the lowest order contributions.

As shown in App. B, for k odd we have $\tilde{\lambda}_n^{(k)} = 0$; for k even the first three terms are given by

$$\tilde{\lambda}_n^{(0)} = \tilde{D}_0 \left(\frac{n\pi}{2} \right)^2, \quad (\text{C8})$$

$$\begin{aligned} \tilde{D}_0 \tilde{\lambda}_n^{(2)} &= \frac{\tilde{E}_1^2}{4} - \tilde{D}_0 \tilde{E}_2 + \frac{1}{16} (-\pi^2 n^2 + 3) \tilde{D}_1^2 \\ &\quad + \frac{1}{12} (\pi^2 n^2 - 6) \tilde{D}_0 \tilde{D}_2 + \frac{1}{2} \tilde{D}_1 \tilde{E}_1, \end{aligned} \quad (\text{C9})$$

$$\begin{aligned} \tilde{D}_0^3 \tilde{\lambda}_n^{(4)} &= \left(\frac{1}{8} - \frac{3}{8\pi^2 n^2} \right) \tilde{D}_1^2 \tilde{E}_1^2 + \left(\frac{1}{3} - \frac{2}{\pi^2 n^2} \right) \tilde{D}_0^2 \tilde{E}_2^2 \\ &\quad + \left(\frac{1}{2} - \frac{3}{\pi^2 n^2} \right) \tilde{D}_0^2 \tilde{E}_1 \tilde{E}_3 + \left(\frac{1}{4} - \frac{3}{4\pi^2 n^2} \right) \tilde{D}_1^3 \tilde{E}_1 \\ &\quad + \left(-\frac{1}{2} + \frac{3}{2\pi^2 n^2} \right) \tilde{D}_0 \tilde{D}_1 \tilde{E}_1 \tilde{E}_2 + \left(-2 + \frac{12}{\pi^2 n^2} \right) \tilde{D}_0^3 \tilde{E}_4 \\ &\quad + \left(-\frac{1}{12} + \frac{1}{2\pi^2 n^2} \right) \tilde{D}_0 \tilde{D}_2 \tilde{E}_1^2 + \left(1 - \frac{3}{2\pi^2 n^2} \right) \tilde{D}_0^2 \tilde{D}_1 \tilde{E}_3 \\ &\quad + \left(-\frac{1}{2} + \frac{3}{2\pi^2 n^2} \right) \tilde{D}_0 \tilde{D}_1^2 \tilde{E}_2 + \left(\frac{2}{3} - \frac{4}{\pi^2 n^2} \right) \tilde{D}_0^2 \tilde{D}_2 \tilde{E}_2 \\ &\quad + \left(-\frac{2}{3} + \frac{5}{2\pi^2 n^2} \right) \tilde{D}_0 \tilde{D}_1 \tilde{D}_2 \tilde{E}_1 + \left(\frac{1}{2} - \frac{3}{\pi^2 n^2} \right) \tilde{D}_0^2 \tilde{D}_3 \tilde{E}_1 \\ &\quad + \left(\frac{3}{32} - \frac{9}{32\pi^2 n^2} - \frac{\pi^2 n^2}{64} \right) \tilde{D}_1^4 \\ &\quad + \left(-\frac{7}{16} + \frac{\pi^2 n^2}{16} + \frac{3}{2\pi^2 n^2} \right) \tilde{D}_0 \tilde{D}_1^2 \tilde{D}_2 \\ &\quad + \left(\frac{1}{4} - \frac{3}{2\pi^2 n^2} - \frac{\pi^2 n^2}{60} \right) \tilde{D}_0^2 \tilde{D}_2^2 \\ &\quad + \left(\frac{5}{8} - \frac{3}{2\pi^2 n^2} - \frac{3\pi^2 n^2}{40} \right) \tilde{D}_0^2 \tilde{D}_1 \tilde{D}_3 \\ &\quad + \left(-1 + \frac{6}{\pi^2 n^2} + \frac{\pi^2 n^2}{20} \right) \tilde{D}_0^3 \tilde{D}_4. \end{aligned} \quad (\text{C10})$$

The perturbative contributions to the eigenfunctions are of the form

$$\begin{aligned} \tilde{\rho}_n^{(k)}(\tilde{x}, \tilde{t}) &= \tilde{Q}_{n,s}^{(k)}(\tilde{x}, \tilde{t}) \cdot \sin \left[n \frac{\pi}{2} (\tilde{x} + 1) \right] \\ &\quad + \tilde{Q}_{n,c}^{(k)}(\tilde{x}, \tilde{t}) \cdot \cos \left[n \frac{\pi}{2} (\tilde{x} + 1) \right], \end{aligned} \quad (\text{C11})$$

where $\tilde{Q}_{n,s}^{(k)}(\tilde{x}, \tilde{t})$, $\tilde{Q}_{n,c}^{(k)}(\tilde{x}, \tilde{t})$ are polynomials in \tilde{x} . To order $\tilde{\epsilon}^2$, these polynomials follow as

$$\tilde{Q}_{n,s}^{(0)}(\tilde{x}) = 1, \quad \tilde{Q}_{n,c}^{(0)}(\tilde{x}) = 0, \quad (\text{C12})$$

$$\tilde{Q}_{n,s}^{(1)}(\tilde{x}) = -\frac{\tilde{x}^2}{4\tilde{D}_0} (2\tilde{E}_1 + 3\tilde{D}_1), \quad (\text{C13})$$

$$\tilde{Q}_{n,c}^{(1)}(\tilde{x}) = \frac{n\pi\tilde{x}}{8\tilde{D}_0} (1 - \tilde{x}^2) \tilde{D}_1, \quad (\text{C14})$$

$$\begin{aligned} \tilde{Q}_{n,s}^{(2)}(\tilde{x}) &= \frac{\tilde{x}}{384\tilde{D}_0^2} \left[48\tilde{x}^2 \tilde{E}_1^2 + 240\tilde{x}^2 \tilde{D}_1 \tilde{E}_1 \right. \\ &\quad + (-24 + 252\tilde{x}^2 - 3\pi^2 n^2 - 3\pi^2 n^2 \tilde{x}^4 + 6\pi^2 n^2 \tilde{x}^2) \tilde{D}_1^2 \\ &\quad \left. - 192\tilde{x}^2 \tilde{D}_0 \tilde{E}_2 + (32 - 288\tilde{x}^2) \tilde{D}_0 \tilde{D}_2 \right], \end{aligned} \quad (\text{C15})$$

$$\tilde{Q}_{n,c}^{(2)}(\tilde{x}) = \frac{\tilde{x}^2 n\pi}{96\tilde{D}_0^2} (1 - \tilde{x}^2) \left[-6\tilde{D}_1 \tilde{E}_1 - 15\tilde{D}_1^2 + 8\tilde{D}_0 \tilde{D}_2 \right], \quad (\text{C16})$$

where the $\tilde{E}_k \equiv \tilde{E}_k(\tilde{t})$, $\tilde{D}_k \equiv \tilde{D}_k(\tilde{t})$ are defined in Eqs. (C4), (C6).

If the diffusivity is independent of position, $D(x) \equiv D_0$, then $\tilde{D}_0 \equiv 1$ and $\tilde{D}_k = 0$ for all $k \geq 1$. In that case, Eqs. (C8-C16) reduce to the corresponding results derived in Ref. [27].

2. Perturbative calculation of the reflecting-boundary steady state and its multiplicative inverse

To evaluate the inner product Eq. (A10) perturbatively, the power-series expansion Eq. (B24) needs to be obtained. The corresponding formal steady state $\tilde{\rho}_{ss}$ of the dimensionless FP operator is for one-dimensional systems given by

$$\tilde{\mathcal{F}}_{\text{app}} \tilde{\rho}_{ss} = \partial_{\tilde{x}} \left[-\tilde{\epsilon} \tilde{a}_{\text{app}} \tilde{\rho}_{ss} + \partial_{\tilde{x}} \left(\tilde{D} \tilde{\rho}_{ss} \right) \right] \equiv 0, \quad (\text{C17})$$

with the boundary conditions

$$\left[-\tilde{\epsilon} \tilde{a}_{\text{app}} \tilde{\rho}_{ss} + \partial_{\tilde{x}} \left(\tilde{D} \tilde{\rho}_{ss} \right) \right] \Big|_{\tilde{x}=\pm 1} = 0. \quad (\text{C18})$$

Integrating Eq. (C17) with respect to \tilde{x} and using Eq. (C18), we obtain

$$\partial_{\tilde{x}} \left(\tilde{D} \tilde{\rho}_{ss} \right) = \frac{\tilde{\epsilon} \tilde{a}_{\text{app}} \tilde{\rho}_{ss}}{\tilde{D}} \left(\tilde{D} \tilde{\rho}_{ss} \right). \quad (\text{C19})$$

The solution to this first-order ODE is

$$\tilde{D}(\tilde{x}) \tilde{\rho}_{ss}(\tilde{x}) = \tilde{D}_0 \exp \left[\int_0^{\tilde{x}} d\tilde{y} \frac{\tilde{\epsilon} \tilde{a}_{\text{app}} \tilde{\rho}_{ss}}{\tilde{D}} \Big|_{\tilde{y}} \right] \quad (\text{C20})$$

where we chose the constant of integration such that $\tilde{\rho}_{ss}(\tilde{x} = 0) = 1$; a different choice corresponds to a rescaling of the inner product. Solving Eq. (C20) for $\tilde{\rho}_{ss}^{-1}(\tilde{x})$ and substituting the power series Eqs. (C3), (C5), we obtain

$$\tilde{\rho}_{ss}^{-1}(\tilde{x}) = \frac{\sum_{k=0}^{\infty} \tilde{\epsilon}^k \tilde{D}_k \tilde{x}^k}{\tilde{D}_0} \exp \left[\int_0^{\tilde{x}} d\tilde{y} \frac{\sum_{k=1}^{\infty} k \tilde{\epsilon}^k \tilde{E}_k \tilde{y}^{k-1}}{\sum_{k=0}^{\infty} \tilde{\epsilon}^k \tilde{D}_k \tilde{y}^k} \right]. \quad (\text{C21})$$

The power-series expansion Eq. (B24) of $\tilde{\rho}_{ss}^{-1}$ is obtained from Eq. (C21) by first expanding the integrand in the exponent to the desired order in $\tilde{\epsilon}$, performing the integral, subsequently expanding both the exponential and the prefactor, and finally their product to the desired order in $\tilde{\epsilon}$. To order $\tilde{\epsilon}^2$, this yields

$$(\tilde{\rho}_{ss}^{-1})^{(0)} = 1, \quad (\tilde{\rho}_{ss}^{-1})^{(1)} = \frac{\tilde{x}}{\tilde{D}_0} (\tilde{E}_1 + \tilde{D}_1), \quad (\text{C22})$$

$$(\tilde{\rho}_{ss}^{-1})^{(2)} = \frac{\tilde{x}^2}{2\tilde{D}_0^2} \left(\tilde{E}_1^2 + \tilde{D}_1 \tilde{E}_1 + 2\tilde{D}_0 \tilde{E}_2 + 2\tilde{D}_0 \tilde{D}_2 \right) \quad (\text{C23})$$

where $\tilde{E}_k \equiv \tilde{E}_k(\tilde{t})$, $\tilde{D}_k \equiv \tilde{D}_k(\tilde{t})$ are defined in Eqs. (C4), (C6).

3. Exit rate to order R^2

Using the perturbative results for the spectrum and instantaneous steady state calculated in Sects. C1, C2, the dimensionless form of the exit rate Eq. (7), which is given by Eq. (A22), is evaluated for $N = 1$. The resulting

terms of the perturbation series are

$$\tilde{\alpha}_{\text{free}}^\varphi = \frac{\pi^2 \tilde{D}_0}{4\tilde{\epsilon}^2}, \quad (\text{C24})$$

$$\begin{aligned} \tilde{D}_0 \tilde{\alpha}^{\varphi,(0)} &= \frac{\tilde{E}_1^2}{4} - \tilde{D}_0 \tilde{E}_2 + \frac{\tilde{D}_1 \tilde{E}_1}{2} \\ &\quad - \left(\frac{\pi^2}{16} - \frac{3}{16} \right) \tilde{D}_1^2 + \left(\frac{\pi^2}{12} - \frac{1}{2} \right) \tilde{D}_0 \tilde{D}_2, \end{aligned} \quad (\text{C25})$$

$$\begin{aligned} \tilde{D}_0^3 \tilde{\alpha}^{\varphi,(2)} &= \left(\frac{1}{8} - \frac{3}{8\pi^2} \right) \tilde{D}_1^2 \tilde{E}_1^2 + \left(\frac{1}{4} - \frac{3}{4\pi^2} \right) \tilde{D}_1^3 \tilde{E}_1 + \left(\frac{3}{32} - \frac{9}{32\pi^2} - \frac{\pi^2}{64} \right) \tilde{D}_1^4 + \left(-\frac{1}{12} + \frac{1}{2\pi^2} \right) \tilde{D}_0 \tilde{D}_2 \tilde{E}_1^2 \\ &\quad + \left(-\frac{1}{2} + \frac{3}{2\pi^2} \right) \tilde{D}_0 \tilde{D}_1 \tilde{E}_1 \tilde{E}_2 + \left(-\frac{2}{3} + \frac{5}{2\pi^2} \right) \tilde{D}_0 \tilde{D}_1 \tilde{D}_2 \tilde{E}_1 + \left(-\frac{1}{2} + \frac{3}{2\pi^2} \right) \tilde{D}_0 \tilde{D}_1^2 \tilde{E}_2 \\ &\quad + \left(-\frac{7}{16} + \frac{\pi^2}{16} + \frac{3}{2\pi^2} \right) \tilde{D}_0 \tilde{D}_1^2 \tilde{D}_2 + \left(\frac{1}{3} - \frac{2}{\pi^2} \right) \tilde{D}_0^2 \tilde{E}_2^2 + \left(\frac{2}{3} - \frac{4}{\pi^2} \right) \tilde{D}_0^2 \tilde{D}_2 \tilde{E}_2 + \left(\frac{1}{4} - \frac{3}{2\pi^2} - \frac{\pi^2}{60} \right) \tilde{D}_0^2 \tilde{D}_2^2 \\ &\quad + \left(\frac{1}{2} - \frac{3}{\pi^2} \right) \tilde{D}_0^2 \tilde{E}_1 \tilde{E}_3 + \left(\frac{1}{2} - \frac{3}{\pi^2} \right) \tilde{D}_0^2 \tilde{D}_3 \tilde{E}_1 + \left(1 - \frac{3}{2\pi^2} \right) \tilde{D}_0^2 \tilde{D}_1 \tilde{E}_3 + \left(\frac{5}{8} - \frac{3}{2\pi^2} - \frac{3\pi^2}{40} \right) \tilde{D}_0^2 \tilde{D}_1 \tilde{D}_3 \\ &\quad + \left(-2 + \frac{12}{\pi^2} \right) \tilde{D}_0^3 \tilde{E}_4 + \left(-1 + \frac{6}{\pi^2} + \frac{\pi^2}{20} \right) \tilde{D}_0^3 \tilde{D}_4 + \left(\frac{1}{3} - \frac{3}{\pi^2} \right) \tilde{D}_0^2 \dot{\tilde{E}}_2 + \left(\frac{1}{6} - \frac{1}{\pi^2} \right) \tilde{D}_0^2 \dot{\tilde{D}}_2 \\ &\quad + \left(-\frac{1}{4} + \frac{2}{\pi^2} \right) \tilde{D}_0 \tilde{E}_1 \dot{\tilde{E}}_1 + \left(-\frac{5}{24} + \frac{7}{4\pi^2} \right) \tilde{D}_0 \tilde{D}_1 \dot{\tilde{E}}_1 + \left(-\frac{7}{24} + \frac{3}{2\pi^2} \right) \tilde{D}_0 \tilde{E}_1 \dot{\tilde{D}}_1 + \left(-\frac{3}{16} + \frac{3}{4\pi^2} \right) \tilde{D}_0 \tilde{D}_1 \dot{\tilde{D}}_1 \\ &\quad + \left(\frac{1}{4} - \frac{2}{\pi^2} \right) \tilde{E}_1^2 \dot{\tilde{D}}_0 + \left(\frac{1}{2} - \frac{13}{4\pi^2} \right) \tilde{D}_1 \tilde{E}_1 \dot{\tilde{D}}_0 + \left(\frac{3}{16} - \frac{3}{4\pi^2} \right) \tilde{D}_1^2 \dot{\tilde{D}}_0 + \left(-\frac{1}{3} + \frac{3}{\pi^2} \right) \tilde{D}_0 \tilde{E}_2 \dot{\tilde{D}}_0 \\ &\quad + \left(-\frac{1}{6} + \frac{1}{\pi^2} \right) \tilde{D}_0 \tilde{D}_2 \dot{\tilde{D}}_0 + \left(-\frac{1}{4} + \frac{2}{\pi^2} \right) \tilde{D}_0 \tilde{E}_1^2 \dot{\tilde{\epsilon}} + \left(-\frac{3}{4} + \frac{4}{\pi^2} \right) \tilde{D}_0 \tilde{D}_1 \tilde{E}_1 \dot{\tilde{\epsilon}} + \left(-\frac{7}{16} + \frac{3}{2\pi^2} \right) \tilde{D}_0 \tilde{D}_1^2 \dot{\tilde{\epsilon}} \\ &\quad + \left(1 - \frac{8}{\pi^2} \right) \tilde{D}_0^2 \tilde{E}_2 \dot{\tilde{\epsilon}} + \left(\frac{2}{3} - \frac{4}{\pi^2} \right) \tilde{D}_0^2 \tilde{D}_2 \dot{\tilde{\epsilon}}, \end{aligned} \quad (\text{C26})$$

where $\tilde{E}_k \equiv \tilde{E}_k(\tilde{t})$, $\tilde{D}_k \equiv \tilde{D}_k(\tilde{t})$ are defined in Eqs. (C4), (C6), and a dot denotes a derivative with respect to \tilde{t} . By substituting the definitions of \tilde{E}_k , \tilde{D}_k , the exit rate is fully expressed in terms of the drift and diffusion of the 1D FPE. In particular, from Eq. (C24) we obtain the steady-state free diffusion exit rate

$$\alpha_{\text{free}}^\varphi = \frac{1}{\tau_D} \tilde{\alpha}_{\text{free}}^\varphi = \frac{\pi^2 D(\varphi(t), t)}{4R(t)^2}, \quad (\text{C27})$$

so that the function f^φ from Eq. (8) is for $N = 1$ given by $f^\varphi(t) = \pi^2 D(\varphi(t), t)/4$ and Eq. (21) follows. The order- R^0 contribution Eq. (22) is obtained by substituting the definitions of \tilde{E}_k , \tilde{D}_k into Eq. (C25) and using the drift and diffusion of the FP Eq. (20).

4. Comparison of small-radius perturbative results to numerical simulations

In Sect. III B we consider the exit rate Eq. (7) to order R^0 for three different scenarios, namely a constant-radius tube, a constant free-diffusion exit rate tube, and the exit rate related to the Stratonovich construction. By comparing our perturbative analytical results to order R^0 with exit rates measured in numerical simulations, we in the present section demonstrate that for all three scenarios, and for the radii considered in Sect. III B, the analytical perturbative exit rate Eq. (7) to order R^0 describes perfectly the actual exit rate.

For the numerical results presented here, the dimensionless form of the 1D FPE (20) with absorbing boundary conditions is simulated using the forward Euler algorithm described in Ref. [27]; from the resulting trajectory, the exit rate is obtained via numerical evaluation of Eq. (18).

Scenario 1: Constant radius. We now compare the an-

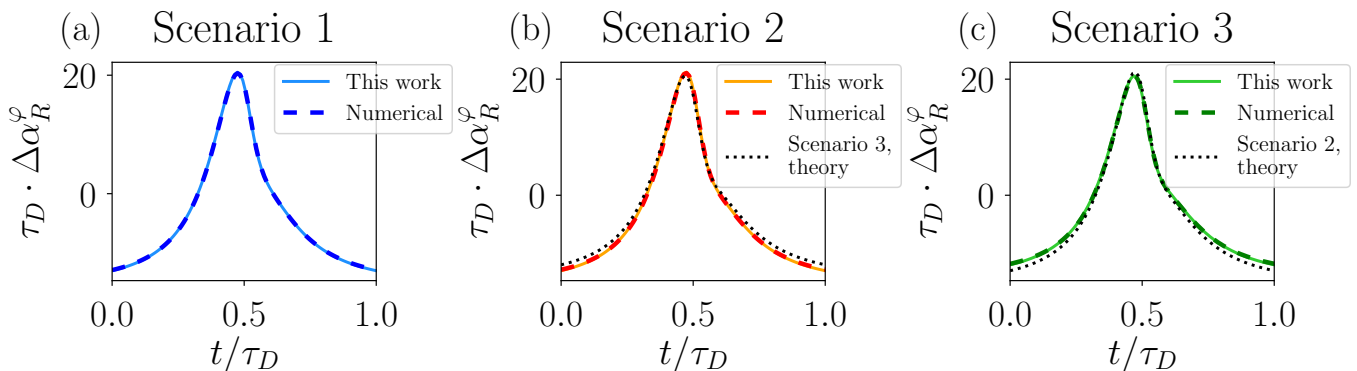


Figure 6. Comparison of theoretical and numerical exit rates for the example system considered in Sect. III and defined in Sect. III A. All subplots compare the difference between exit rates measured in numerical simulations and free-diffusion exit rates, Eq. (C28), to the corresponding theoretical prediction $\alpha^{\varphi,(0)}$. For numerical results, the dimensionless form of the 1D FPE (20) with absorbing boundary conditions is simulated using the algorithm described in Ref. [27]; from the resulting trajectory, the exit rate is obtained via numerical evaluation of Eq. (18). Subplot (a) shows results for constant tube radius (scenario 1). The solid line depicts the theoretical result Eq. (28), the dashed line is obtained by measuring the exit rate in numerical simulations and subtracting Eq. (27). Subplot (b) considers a time-dependent tube radius such that the free-diffusion exit rate is constant (scenario 2). The solid line depicts the theoretical result Eq. (30), the dashed line is obtained by measuring the exit rate in numerical simulations and subtracting Eq. (29). For comparison, the Stratonovich Lagrangian Eq. (32) is shown as dotted line. Subplot (c) shows results for the Stratonovich construction (scenario 3). The solid line depicts the theoretical result Eq. (32), the dashed line is obtained by measuring the exit rate in numerical simulations and subtracting the first term from Eq. (34). For comparison, the constant free-diffusion Lagrangian Eq. (30) is shown as dotted line.

analytical exit rate Eqs. (7), (27), (28), to numerical results. In Fig. 6 (a), we compare the deviation of the numerical exit rate from the free-diffusion rate Eq. (27), i.e.

$$\Delta \alpha_R^\varphi(t) = \alpha_R^\varphi(t) - \alpha_{\text{free}}^\varphi(t), \quad (\text{C28})$$

with the Lagrangian Eq. (28). As can be seen, the numerical curve agrees perfectly with $\mathcal{L}_1^{\varphi,(0)}$, showing that for the radius $\bar{\epsilon} \equiv R_0/L = 0.1$, the numerical exit rate is described by the perturbative result Eqs. (7), (27), (28).

Scenario 2: Constant free-diffusion exit rate. In Fig. 6 (b) we compare Eq. (C28), the deviation of the numerical

exit rate from the free-diffusion exit rate Eq. (29), with the Lagrangian Eq. (30). The perfect agreement between simulations and theory shows that also in scenario 2, the perturbative expansion Eq. (7) describes the actual exit rate from the small-radius tube.

Scenario 3: Stratonovich Lagrangian. In Fig. 6 (c) we compare the theoretical exit rate Eq. (34) to results from numerical simulations of the FPE in the y -coordinate defined in Eq. (33). As for scenarios 1 and 2, we find perfect agreement between perturbative and numerical exit rates, showing that our perturbative expansion describes the exit rate for the tube radius considered.

-
- [1] Norbert Wiener, “Differential-Space,” *Journal of Mathematics and Physics* **2**, 131–174 (1923).
 [2] L. Onsager and S. Machlup, “Fluctuations and Irreversible Processes,” *Physical Review* **91**, 1505–1512 (1953).
 [3] Ruslan Leontievich Stratonovich, “On the probability functional of diffusion processes,” *Selected Trans. in Math. Stat. Prob* **10**, 273 (1971).
 [4] Detlef Dürr and Alexander Bach, “The Onsager-Machlup function as Lagrangian for the most probable path of a diffusion process,” *Communications in Mathematical Physics* **60**, 153–170 (1978).
 [5] Takahiko Fujita and Shin-ichi Kotani, “The Onsager-Machlup function for diffusion processes,” *Journal of Mathematics of Kyoto University* **22**, 115–130 (1982).
 [6] W. Horsthemke and A. Bach, “Onsager-Machlup Function for one dimensional nonlinear diffusion processes,” *Zeitschrift für Physik B Condensed Matter and Quanta* **22**, 189–192 (1975).
 [7] H. Ito, “Probabilistic Construction of Lagrangean of Diffusion Process and Its Application,” *Progress of Theoretical Physics* **59**, 725–741 (1978).
 [8] Y. Takahashi and S. Watanabe, “The probability functionals (Onsager-machlup functions) of diffusion processes,” in *Stochastic Integrals*, Vol. 851, edited by David Williams (Springer Berlin Heidelberg, Berlin, Heidelberg, 1981) pp. 433–463.
 [9] Nobuyuki Ikeda and Shinzo Watanabe, *Stochastic differential Equations and diffusion processes*, 2nd ed., North-Holland mathematical Library No. 24 (North-Holland [u.a.], Amsterdam, 1989) oCLC: 20080337.
 [10] Robert Graham, “Path integral formulation of general diffusion processes,” *Zeitschrift für Physik B Condensed Matter and Quanta* **26**, 281–290 (1977).

- [11] F. Langouche, D. Roekaerts, and E. Tirapegui, “Functional integral methods for stochastic fields,” *Physica A: Statistical Mechanics and its Applications* **95**, 252–274 (1979).
- [12] H. Dekker, “On the path integral for diffusion in curved spaces,” *Physica A: Statistical Mechanics and its Applications* **103**, 586–596 (1980).
- [13] Markus F Weber and Erwin Frey, “Master equations and the theory of stochastic path integrals,” *Reports on Progress in Physics* **80**, 046601 (2017).
- [14] C. Wissel, “Manifolds of equivalent path integral solutions of the Fokker-Planck equation,” *Zeitschrift für Physik B Condensed Matter and Quanta* **35**, 185–191 (1979).
- [15] Artur B. Adib, “Stochastic Actions for Diffusive Dynamics: Reweighting, Sampling, and Minimization,” *The Journal of Physical Chemistry B* **112**, 5910–5916 (2008).
- [16] Leticia F Cugliandolo, Vivien Lecomte, and Frédéric van Wijland, “Building a path-integral calculus: a covariant discretization approach,” *Journal of Physics A: Mathematical and Theoretical* **52**, 50LT01 (2019).
- [17] M. I. Dykman, P. V. E. McClintock, V. N. Smelyanski, N. D. Stein, and N. G. Stocks, “Optimal paths and the prehistory problem for large fluctuations in noise-driven systems,” *Physical Review Letters* **68**, 2718–2721 (1992).
- [18] D G Luchinsky, P V E McClintock, and M I Dykman, “Analogue studies of nonlinear systems,” *Reports on Progress in Physics* **61**, 889–997 (1998).
- [19] Weinan E, Weiqing Ren, and Eric Vanden-Eijnden, “String method for the study of rare events,” *Physical Review B* **66**, 052301 (2002).
- [20] Weiqing Ren, Eric Vanden-Eijnden, Paul Maragakis, and Weinan E, “Transition pathways in complex systems: Application of the finite-temperature string method to the alanine dipeptide,” *The Journal of Chemical Physics* **123**, 134109 (2005).
- [21] Weinan E, Weiqing Ren, and Eric Vanden-Eijnden, “Transition pathways in complex systems: Reaction coordinates, isocommittor surfaces, and transition tubes,” *Chemical Physics Letters* **413**, 242–247 (2005).
- [22] H. B. Chan, M. I. Dykman, and C. Stambaugh, “Paths of Fluctuation Induced Switching,” *Physical Review Letters* **100** (2008), 10.1103/PhysRevLett.100.130602.
- [23] Hiroshi Fujisaki, Motoyuki Shiga, and Akinori Kidera, “Onsager–Machlup action-based path sampling and its combination with replica exchange for diffusive and multiple pathways,” *The Journal of Chemical Physics* **132**, 134101 (2010).
- [24] Christian Maes and Karel Netočný, “Time-Reversal and Entropy,” *Journal of Statistical Physics* **110**, 269–310 (2003).
- [25] Udo Seifert, “Entropy production along a stochastic trajectory and an integral fluctuation theorem,” *Physical Review Letters* **95**, 040602 (2005), arXiv: cond-mat/0503686.
- [26] Udo Seifert, “Stochastic thermodynamics, fluctuation theorems, and molecular machines,” *Reports on Progress in Physics* **75**, 126001 (2012), arXiv: 1205.4176.
- [27] Julian Kappler and Ronjoy Adhikari, “Stochastic action for tubes: Connecting path probabilities to measurement,” *Physical Review Research* **2** (2020), 10.1103/PhysRevResearch.2.023407.
- [28] Jannes Gladrow, Ulrich F. Keyser, R. Adhikari, and Julian Kappler, “Direct experimental measurement of relative path probabilities and stochastic actions,” arXiv:2006.16820 [cond-mat, physics:physics] (2020), arXiv: 2006.16820.
- [29] N. G. van Kampen, *Stochastic processes in physics and chemistry*, 3rd ed., North-Holland personal library (Elsevier, Amsterdam ; Boston, 2007) oCLC: ocm81453662.
- [30] Gerhard Hummer, “Position-dependent diffusion coefficients and free energies from Bayesian analysis of equilibrium and replica molecular dynamics simulations,” *New Journal of Physics* **7**, 34–34 (2005).
- [31] Felix Sedlmeier, Yann von Hansen, Liang Mengyu, Dominik Horinek, and Roland R. Netz, “Water Dynamics at Interfaces and Solutes: Disentangling Free Energy and Diffusivity Contributions,” *Journal of Statistical Physics* **145**, 240–252 (2011).
- [32] Alexander Berezhkovskii and Attila Szabo, “Time scale separation leads to position-dependent diffusion along a slow coordinate,” *The Journal of Chemical Physics* **135**, 074108 (2011).
- [33] Stefano Bo, Soon Hoe Lim, and Ralf Eichhorn, “Functionals in stochastic thermodynamics: how to interpret stochastic integrals,” *Journal of Statistical Mechanics: Theory and Experiment* **2019**, 084005 (2019).
- [34] T. J. Murphy and J. L. Aguirre, “Brownian Motion of N Interacting Particles. I. Extension of the Einstein Diffusion Relation to the N-Particle Case,” *The Journal of Chemical Physics* **57**, 2098–2104 (1972).
- [35] Gerald Wilemski, “On the derivation of Smoluchowski equations with corrections in the classical theory of Brownian motion,” *Journal of Statistical Physics* **14**, 153–169 (1976).
- [36] Rajesh Singh and R. Adhikari, “Fluctuating hydrodynamics and the Brownian motion of an active colloid near a wall,” *European Journal of Computational Mechanics* **26**, 78–97 (2017).
- [37] A D Ventsel’ and M I Freidlin, “On small random perturbations of dynamical systems,” *Russian Mathematical Surveys* **25**, 1–55 (1970).
- [38] Julian Kappler and Ronjoy Adhikari, “Irreversibility and entropy production along paths as a difference of tubular exit rates,” arXiv:2007.11639 [cond-mat, physics:physics] (2020), arXiv: 2007.11639.
- [39] Crispin W. Gardiner, *Stochastic methods: a handbook for the natural and social sciences*, 4th ed., Springer series in synergetics (Springer, Berlin, 2009).
- [40] Ofer Zeitouni, “On the Onsager-Machlup Functional of Diffusion Processes Around Non C2 Curves,” *The Annals of Probability* **17**, 1037–1054 (1989).
- [41] Leslie E. Ballentine, *Quantum mechanics: a modern development*, repr ed. (World Scientific, Singapore, 2010) oCLC: 846445677.
- [42] N. G. van Kampen, “Itô versus Stratonovich,” *Journal of Statistical Physics* **24**, 175–187 (1981).
- [43] J. M. Sancho, M. San Miguel, and D. Dürr, “Adiabatic elimination for systems of Brownian particles with nonconstant damping coefficients,” *Journal of Statistical Physics* **28**, 291–305 (1982).
- [44] Nikolaus Hansen, Youhei Akimoto, and Petr Baudis, “CMA-ES/pycma: r2.7.0,” (2019), 10.5281/ZENODO.2559634, publisher: Zenodo.
- [45] D. S. Grebenkov and B.-T. Nguyen, “Geometrical Structure of Laplacian Eigenfunctions,” *SIAM Review* **55**, 601–667 (2013).